NTNU

Norwegian University of
Science and Technology

Methodology for Detecting and Interpreting Instantaneous Frequencies in Stand-alone Microgrids

An Application of the Hilbert Huang
Transform on Electrical Networks

Benedikt Hillenbrand

Master of Science in Electric Power Engineering
Submission date: June 2017
Supervisor: Marta Maria Cabrera Molinas, ITK

Norwegian University of Science and Technology
Department of Engineering Cybernetics

Abstract

Following the tile, this thesis seeks to find a methodology for detecting and interpreting instantaneous frequencies in stand-alone microgrids. This is not a novel exercise for scientists to do but it bears potential to be improved by making use of a new method - the Empirical Mode Decomposition (EMD). The EMD is a non-linear algorithm that separates any oscillating signal into mono-components, leaving space for time-varying amplitude and -frequency of the so called Intrinsic Mode Functions.

To start with, a brief introduction to stand-alone microgrids is given. Microgrids are considered to be driven by renewable energy sources such as e.g. solar-panels which make electrical power converter necessary to transform the produced energy from DC to AC. The control of the power converters plays the lead role in shaping voltage and current waveforms of the network while no other traditional type of rotating generators are assumed. The imitation of synchronous machine behaviour, however is a favoured method to control converters because traditional machines have certain inherent advantageous physical properties. The power-balance (load-/supply mismatch) and the fundamental frequency of the network (usually 50 Hz or 60 Hz) are set into a backhanded relationship so that changes in the consumed, or generated power leads to a changing fundamental frequency. The impact of fast changing solar power (e.g. reasoned by non-steady solar irradiance - clouds) is obvious and as a follow-up from the converter control it can lead to a supply-fluctuation and violation of the fundamental frequency. Deterioration of the power quality and wrong statements on the actual network status due to improper measurement equipment can follow and are part of the investigation of this thesis. The EMD plays a key-role, as it shows certain advantages against the widely used Fast Fourier Transform in handling non-linear, non-steady signal. The core of the thesis deals with the analysis of voltage and current measurements from stand-alone microgrid, 3-phase systems. Focusing on detecting the true composition of the measured signal, several methods, based on analysis of the raw measurements, combined 3-phase rotating space vectors for voltages and currents and instantaneous power are developed. The developed methods are applied to data, recorded at a marine vessel during sea-voyage. The system on board the ship has certain similarities to previous explained onshore networks, as the balance between generated and consumed power is dynamic. In the ship, the generation is relatively steady but the load (electrical propulsion) varies vastly.

Acknowledgement

Marta Molinas, for supervising, trusting and pushing.
Geir Kulia, for many helpful discussions, the basic EMD-code and his work in Bhutan, together with Hakon Duus.
For being available for spontaneous questions and fruitful discussions: Amin Mohammad, Jing Lyu, Paula Garcia Rosa, Eneko Unamuno, Victoria Gasca, Maximiliano Bueno Lopez, Noe Barrera Gallegos.

Contents

Motivation

The motivation of one to perform work is the most important factor for a good work. For the completion of this thesis, there were a couple of motivations from different nature that were important to complete the project.

In 2010, the country of Bhutan announced to electrify its population in rural areas by 2013 to 100 % by means of remote micro-grids [1]. In 2014 this goal was achieved to 95 % as shown in fig. 1. Work done in this thesis is not only directed to the Bhutan project, but the project shows that many people depend on the technology that is used to built isolated electrical networks. Previous to this thesis, two students dedicated their MSc project to a case in Bhutan [2, 3] and this is to continue on that track.

The Question may arise "Why renewable electricity in developing countries?". The answer is diverse and can be approached with referring to medical purposes (cooling medicine, operation of medical equipment, ... [4]), modern means of education, lighting without releasing toxic combustion products or giving people the opportunity to connect by modern means of communication. These are examples, linked to the United Nations Development Programme (UNDP), goal 7 "ensure access to affordable, reliable, sustainable and modern energy for all" and 13 "take urgent action to combat climate change and its impacts". This thesis does not aim to provide power to people that do not have it yet, but it focuses on starting a discussion on power quality of already existing and future systems as losses and reliability of equipment strongly depends on the quality of voltages and currents of the network. Stand-alone microgrids are arising and with them the need for reliable

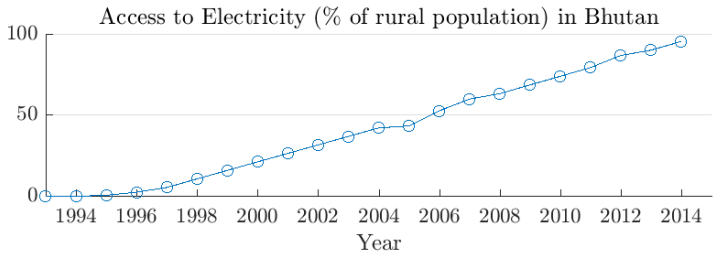

Figure 1: Data from the World Bank. Access to Energy of the Bhutanese population, living in rural areas.

analysis methods. This is to evaluate their performance, improve reliability and finally avoid black outs by being aware of the momentary system state.

First it is essential to show the actual state of the system which is often not possible with conventional equipment. In a second step, that would be the continuation of the thesis, the reasons for weak power quality must be found to mitigate or eliminate them.

The Huang Hilbert Transform (HHT) is a non-linear method to investigate non-stationary oscillating signal. It comprises an algorithm that is used in many applications (weather data, medical data, ...) but hasn't found its way to applications in electrical power systems. However, as voltages and currents are sinusoidal oscillating signals, highly distorted by non-linear, time-variant loads in real live, the HHT promises to be an analysis method with high potential in that case. In the resent years, many publications addressed the properties of the method with an mathematical/statistically approach and ideas to overcome certain disadvantages have been developed. A motivation of the author is to merge existing evaluation methods for electrical systems with the Empirical Mode Decomposition (EMD).

All steps require expensive equipment. Once money comes into play, development countries are restricted in their means and high quality analysis (especially by the countries own research teams) is unlikely to happen. The work within the thesis is done to be part of a analysis method that will be licensed under open access. Thus being available to everyone, including institutions in developing countries. As shown by John H. Barton in [5], the transfer of knowledge to those regions of the world can be done by three modes. First to supply products, second to make licenses available and enable the countries to produce their own products and at last to support research, conducted in the respective country. Capitalistic countries would prefer the modes in the order as they are listed. Developing countries would favour them in a contrary order for being independent on long terms. The project can not address modes 1 and 3, but by licensing the results under open access, ease the use by people in need for it. Barton in 2007 mentions the risk of inaccessible technologies: "Major developing country concerns in future market for energy: Possible difficulties in obtaining advanced intellectual property-protected technologies" [5].

Chapter 1

Introduction

The fundamental frequency of electrical systems depends on the power balance between the supply and the load. In case the two sides are in perfect balance, the frequency will be at it's exact definition. This is either 50 Hz or 60 Hz in most networks. If the balance is lost, by either a sudden change in load or supply, the fundamental frequency will be violated and must be restored by control measures. This is how classical networks, based on rotating generators (e.g. driven by steam) work and how the control of state-of-the-art power electronic converters in switch mode is organized. Power electronic converters however do not have inherent inertia as known from classical machines and the variation of the fundamental frequency consequently is greater. This can have certain impacts on the connected equipment, but also challenges measurement equipment that is designed to be used in systems with slow changing fundamental frequency.

The thesis comprises basic research on the usage of the EMD in the analysis of strongly distorted signal.

The thesis is divided in three major parts. At first, the basic theories and mature control methods are derived and explained. In a second step, the novel methodologies to analyze power, based on a combination of classical methods and the EMD are explained. By testing the new methods on measurement signal from a marine vessel, results are analyzed in the the last part. The analysis focuses on the analysis of voltages and currents, but the analysis of instantaneous power exceeds the dimension of the thesis. Therefore, beyond the thesis, a conference paper (title: Impact of Time Varying Angular Frequency on the Separation of Instantaneous Power Components in Stand-alone Power Systems) will be presented at ICCEP in June 2017, addressing the application of the EMD in shunt active filter to minimize power exchange between lines. If correctly implemented, the compensated currents only contribute in transferring active power from one to another point in the network.

The nomenclature of Akagi is used when talking about electrical data and networks. Norden Huangs paper on the EMD [6] coins the wording when it comes to EMD and signal analysis.

Chapter 2

Research

This Chapter explains the possible origins of fundamental frequency variation based on a study of power converter control. The impact of extensive polluted, non-stationary signal waveforms to measurement equipment in remote 3-phase power networks is also explained. The chapter further shows the state-of-the-art measurement equipment including a discussion on their limitations and gives an introduction to methods that can be used for future signal analysis. A strong emphasis is laid on taking as less as possible mathematical simplifications. Variables (e.g. frequency and amplitude) are assumed to be time-varying.

This chapter will provide the reader with the theories and methods that are used in the Methodology chapter in order to detect and to prove the existence of fundamental frequency fluctuation in rural networks in island mode.

2.1 Power Electronic Converter Control

There are many power electronic converters in a modern power system and even more methods on how they can be controlled. Converters are used to rectify or invert energy because the generation unit might deliver, or the load might require direct current and the transmission system is based on alternating current for most cases. More applications arise as power electronic converter in switch mode offer good controlability. Originally used only for low power applications, the semiconductor-based equipment reached high power applications during the last decades and is responsible for transforming at high power levels.

The major energy flow in small power grids (e.g. as in developing countries) is already completely handled by power electronic converters. This is, because the main energy is supplied by e.g. PV-cells and needs to be inverted. No rotating machine with its inertia is present any more. The development can be found more and more in bigger grids as the amount of renewable energy and non-linear loads is increasing and classical machines are responsible for less of the total generated power.

In classical systems, the control hierarchy is classified into three levels (Ma-

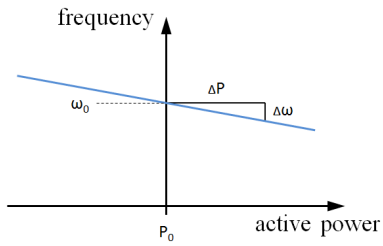

Figure 2.1: Droop control. Active power generation versus frequency variation.

chowski et al. [7]) where the time constants that are addressed by the levels increase from the primary to the tertiary control level.

- Primary Control (Power balance)
- Secondary control (Total power production/sharing)
- Tertiary Control (Economic optimization)

The primary- and secondary control levels are determined by the inherent properties of electrical machines. The droop control. The primary control is keeping the network frequency stable and the secondary control keeps it at its defined fundamental (50 Hz or 60 Hz). If the frequency increases, the consumed power will be decreased as shown in fig. 2.1. Hence, both sides of the equilibrium are frequency depending and can cause frequency fluctuation. The slope of the droop determines how much of the total power is supplied by single generation units. Each Unit has its own droop characteristics and no communication is required to manage how the total load is distributed among the single generation units. The fundamental frequency is the communication channel which is available to every source connected to the grid.

Certain publications are devoted to the control of power electronic converter [8, 9, 10, 11]. Rocabert et al. [9] classifies the control strategies for power converters into 3 classes.

- Grid-forming: AC voltage and frequency are controlled
- Grid-feeding: Active and reactive power are controlled
- Grid-supporting: Two different arrangements of the control scheme are possible, acting either as a Grid-forming, or -feeding converter.

The grid-forming converter topology is suitable for operation in island mode of an micro-grid. The grid-feeding converter topology requires a power source that shapes the voltage of the network and is therefore only suitable in grid-connected mode or in parallel to an respective grid-forming converter.

2.2 Frequency Variation in Electrical Networks

As explained in the previous chapter, frequency variation is caused by a power imbalance between supplied and demanded energy. If both sides are stationary and equal, the frequency remains constant. Demand fluctuations can be explained by loads being switched or controlled so that the total power consumption of a system varies. Supply fluctuations happen to appear with renewable energy sources like solar irradiance, wind, ocean-waves, etc. and have the same effect on the frequency as demand fluctuations. The inverter output (voltage- and current waveforms) depends on one hand and to a major share on the control algorithm that gives the gating signal to the power electronic switches and on the other hand on the load side characteristics.

Beside the power imbalance, there is a possibility of interaction between controllers within a complex network with multiple generation units. This interaction might also lead to frequency variations as been observed in networks with classical (rotating) generation units [7]. Care must be taken to avoid oscillation modes.

2.2.1 Solar Power

Solar power is a major source for electrical energy in rural areas. The fact that it is easy to harness and available at nearly every place on earth started a development of governmental subsidies and technology that lead to mass production and a fast decrease in prices for equipment that is predicted to continue [12].

Still, solar power is a highly non-continuous source of energy. The Japanese company *Chubu* explains the impact of PV power variation in electricity networks with a big share of solar energy [13]. Small clouds don't have any influence because the interruptions smoothen out in the sum of widely distributed PV-panels. Weather changes have a bigger (but slower) impact as the total production changes significantly. Weather forecast can be used to control classical energy carriers in order to compensate for the variation of solar-based generation. In case of a small isolated microgrid however, shading on the solar panel has a big impact on the total generation of the grid. Batteries (or other energy storage means) must be used to compensate for this. Fig. 2.2 shows the generation from a solar panel during a cloudy day.

For a simulation of a PV-based electrical network with focus on fundamental frequency fluctuation, not only the load variation, but also the impact of generation variation should be considered. For this, data on solar irradiance with a sample rate in the range of seconds is required for being able to investigate the fundamental frequency fluctuation. Two methods are available to obtain irradiance data. On one hand, one can use data which is made available by several different organizations, based on satellite measurements. These are *PVGis* (monthly data), *HelioClim-3* database (minutely detailed), *S@tel-light* (monthly data) and more. Most of these organizations however do not support data with a good enough time-resolution. On the other hand, one can record irradiance data onsite by means of a *Pyranometer*. This allows higher time-resolution and more specific seasonal on-site information if carried out for long time periods to cover the cycle of a whole year but requires

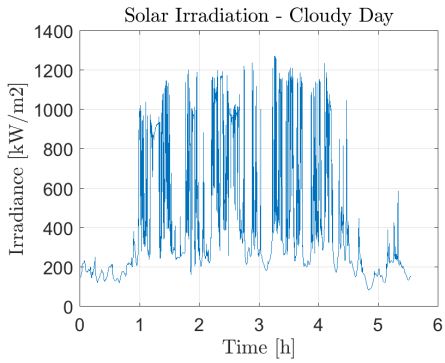

Figure 2.2: Strongly fluctuating solar irradiance measured in Switzerland at a cloudy day. X-axis does not match actual day time, but serves as a time scale. Data acquired by EPFL, Lausanne, Switzerland.

Table 2.1: Comparing the suitability of renewable energy sources for electricity generation.

Energy Source	Intermittency	Controllability
Solar	High	No
Wind	High	No
Hydro	Low	Partly
Biomass	Low	Yes
Diesel	Low	Yes

a physical measurement. The data obtained for fig. 2.2 is based on this method.

2.2.2 Other Energy Sources

Besides solar power, other energy sources are implemented or show potential to be used to feed rural networks. Wind power, hydro power, biomass and diesel are those possible sources [14, 15]. In regards to the supply variation, solar and wind power are not the optimal choice. Due to their high intermittency and low controllability they require energy storage methods to be deployed as a major source for energy in a network. However, they have the advantage of being widely available. Tab. 2.1 shows an overview on several widely used energy sources.

2.2.3 Load Control

The second method to match the supply/demand curve of electrical power is to adjust the consumption to the available energy. This might be an option if the load is controllable. One example is controlling the energy consumption of electrical cooling/heating as the long time-constant of the physical system does not require permanent electrical energy. An improvement of thermal isolation could improve

these devices for the purpose of serving as controllable loads. Depending on the consumers in the network, load control might be an option.

2.2.4 Energy Storage

If the supply/demand curves do not match and can't be fitted, energy storage is required. In the key findings of the International Off-Grid Renewable Energy Conference & Exhibition (IOREC), 2014 a statement on the necessity of energy storage is made: "Control systems can accommodate up to 60% PV penetration without the need for storage. However, van Butselaar commented: "Load profiles define if you have to use storage or don't have to use storage.""[15].

Load-leveling and load-tracking are two terms that describe methods to use energy storage to match supply and demand in a isolated network [9]. Assuming a constant supply and a fluctuating load, the load-leveling approach uses e.g. a battery to smoothen the load profile. In case of load-tracking, the power supply is equipped with energy storage so that a fluctuating demand profile can be followed. The question arises, if batteries can lead to a totally stationary fundamental frequency by perfectly compensating the supply/demand mismatch. As the fundamental frequency serves as the communication channel to spread information on the power balance (droop control), there is a need for deviation from the fundamental frequency to make the controller of a storage element act. Following, the frequency variation is assumed to be mitigated but not extinguished. It depends on the control algorithm and the physical limits (how fast can energy be stored or released) of the storage element. Hydro Storage, batteries or capacitors are possible storage elements, where they are listed in order of increasing price/kWh and decreasing rate of energy-deployment. Energy storage will not perfectly flatten the fluctuation of the fundamental frequency but makes the operation of solar-powered systems possible. A big enough storage should be installed, to last for expected down-times of solar energy.

An interesting study case is the *solar island*, a project conducted by the company *SolarCity*. An island which is supplied by solar power (1.4 MW) and has energy storage (6 MWh) that is meant to last for three consecutive days. The supply and demand is decoupled by the big storage. In most remote networks in developing countries however there is not enough financial means for such dimensions of batteries. The interest of strong partners is required.

2.3 Performance Evaluation of Measurement Equipment

Measuring is the way how an, eventually previously simulated, system can be verified. To get information on effects that might have not been considered during simulation, the measurements should assume as less as possible assumptions (e.g. stationary frequency) from the system and leave room for unsuspected findings.

Starting with this attitude, some weaknesses in conventional definitions for power systems can be found. Typically voltages and currents are either assumed

to be sinusoidal (in very simplified networks) or to consist of a superposition of perfectly sinusoidal components that can be separated by means of (Fast) Fourier Analysis. However, Fourier Analysis shows weaknesses when it is applied to signal that is measured in networks with fast changing fundamental frequency or amplitude. It tries to reconstruct the given signal with perfect sinusoids only and does not allow frequency variation. The Fast Fourier Transform is an adapted version of the Fourier Transform that takes small portions of the signal with a integer-multiple of the period from the fundamental frequency and copies these bits several times so that the conventional (Discrete) Fourier Transform can be applied to it. The EMD does not expect perfectly sinusoidal components.

2.3.1 Classical Power definition and Fourier Transformation

Mohan et al. [16] work with the classical power definition for single phase systems that is valid in steady state. Power is defined based on the Rout Mean Square (RMS) value of voltages and currents which are recurring at a period of T. The basic definition of (instantaneous) power p in equ. 2.1 becomes a stationary value P, defined in equ. 2.3. Capitals indicate RMS values and small letters time-varying values. ϕ corresponds to the phase shift between voltage and current and is used to calculate the Displacement Power Factor (DPF) as in 2.2.

$$p = vi \tag{2.1}$$

$$DPF = cos\,(\phi) \tag{2.2}$$

$$P = \frac{1}{T}\int_0^T vi\,dt = VI \cdot cos\,(\phi) \tag{2.3}$$

To apply the classical power definition to non-sinusoidal current waveforms in steady state, Fourier transformation is used. It separates the fundamental current component from disturbances and the Total Harmonic Distortion (THD) as in equ. 2.4 can be calculated. The voltages are assumed to be sinusoidal with negligible distortion. Equ. 2.5 shows the average power for non-sinusoidal current waveforms.

$$THD_i = \frac{I_{dis}}{I_{s1}} = \sqrt{\sum_{h\neq 1} \frac{I_{sh}^2}{I_{s1}^2}} \tag{2.4}$$

With I_{dis} being the distortion current and I_{s1} the fundamental component of the current. I_{sh} is the harmonic content at the h^{th} multiple of the fundamental frequency. The i in THD_i indicates that the THD corresponds to the current signal.

$$P = VI \cdot \frac{I_{s1}}{I_s} \cdot DPF = VI \cdot \frac{1}{\sqrt{1 + THD_i^2}} \cdot DPF \tag{2.5}$$

In steady state, this definitions are of great importance. However, if the system can not be assumed to be in steady state for long, the definitions need to be handled with care. The main concern is about the Fourier transformation not being able to separate the frequency modes correctly.

Disadvantage of using Fourier transformation on signal with varying fundamental frequency: For systems in stationary conditions, the Discrete Fourier Transform (DFT) can be used to separate frequency components (modes) the whole signal is analyzed at a time. If the system-conditions (especially the fundamental frequency) changes slowly, the power can be approximated by using Fast Fourier Transform (FFT). In comparison to the DFT, the FFT adds an additional time-axis to the frequency- and amplitude- properties of modes. This is possible by evaluating small bits of the total signal at a time. The FFT takes bits of length, corresponding to integer-multiple periods of the fundamental frequency, and copies the bits several times to obtain a longer signal onto which the DFT is applied. After evaluation of this small part of the signal, the fundamental frequency is analyzed again e.g. by means of an Phase Locked Loop (PLL) and a new bit is extracted, copied and the DFT applied. To make sure to always take bits of the correct length of multiple fundamental period, often zero-crossings are used to indicate the periods. The FFT can get disturbed by several effects, such as

- Fast changing fundamental frequency
- High frequency modes at a decimal multiple of the fundamental
- Additional zero-crossings during one cycle of the fundamental frequency in the case of strong-, high frequency harmonic component
- Artifacts such as spikes or temporarily high frequency modes

The measuring window (with a length of a integer multiple of the fundamental frequency) of the FFT needs to be adjusted to the actual fundamental frequency. If that is not done properly, frequency leakage will occur. Several window setups (rectangular, Hamming, Blackman, ...) can be found in the literature [17]. Tarasiuk et al. [18, 19] introduces “coherent sampling” to overcome the problems from adjusting the window size to the fundamental frequency. The EMD as part of the Hilbert Huang Transform (HHT) does not rely on window sizing and can be applied to the whole data-set at a time, similar to the DFT, however, with the advantage of tolerating and giving correct information on time varying frequency.

2.3.2 Instantaneous Power

The instantaneous power theory introduced by Akagi [20] is a new definition of power in 3-phase systems. The major difference to the classical definition is that the measured voltages and currents are not split up by Fourier transform but instantaneous measurements are used to obtain real- and imaginary-power. The real

power can be split up in an average and oscillating part and represents power transfer along e.g. a transmission line. The imaginary part represents power transfer between the three phases only and does not contribute in power transmission. Instead of investigating the sum of single phase power from the classical approach, the instantaneous power defined by Akagi shows details on the 3-phase system that are not observed with before.

The instantaneous power can be calculated in different reference frames (details on reference frames in chapter 2.4.2). Equation 2.6 to 2.8 show the calculation of the real power in abc, $\alpha\beta$ and dq-reference frame respectively. The subscripts identify in which reference frame the calculation is performed. p corresponds to real power and q to imaginary power.

$$p_{inst,abc} = v_a \cdot i_a + v_b \cdot i_b + v_c \cdot i_c \tag{2.6}$$

$$p_{inst,\alpha\beta} = v_\alpha \cdot i_\alpha + v_\beta \cdot i_\beta + v_0 \cdot i_0 \tag{2.7}$$

$$p_{inst,dq} = v_d \cdot i_d + v_q \cdot i_q + v_0 \cdot i_0 \tag{2.8}$$

The equations for calculating imaginary power in the three reference frames are given in 2.9 to 2.11.

$$q_{inst,abc} = \frac{1}{\sqrt{3}} \left[(v_a - v_b) \cdot i_c + (v_b - v_c) \cdot i_a + (v_c - v_a) \cdot i_b \right] \tag{2.9}$$

$$q_{inst,\alpha\beta} = v_\beta \cdot i_\alpha - v_\alpha \cdot i_\beta \tag{2.10}$$

$$q_{inst,dq} = v_q \cdot i_d - v_d \cdot i_q \tag{2.11}$$

Oscillation modes on instantaneous real power: As the instantaneous real power is calculated by multiplying raw measurement signal, possibly including a variety of oscillation-modes, the obtained signal is not constant, but oscillating at different frequency modes. There are different reasons for real power oscillation that can be derived analytically. At first, oscillations in measurements do not lead to instantaneous power oscillations when they occur at the same frequency between voltages and currents and $2\phi/3$ phase shifted between the 3 phases of the network. However, if only present in the currents, but not the voltages, a oscillation mode at e.g. 45 Hz, will lead to a 5 Hz, or 95 Hz oscillation mode in the instantaneous power, depending on the sequence (positive or negative). This is visualized in fig. 2.3. Other than oscillation modes on the voltage or current measurements, two more reasons are identified to lead to instantaneous real power oscillation. On one side, a negative sequence at the fundamental frequency of either voltage or current or on the other side, an offset of one or multiple measurements.

Summarized, there are multiple reasons for instantaneous real power oscillations. When real measurements are analyzed and the system, where the measurements are taken is not known, it is therefore difficult to draw conclusions of the

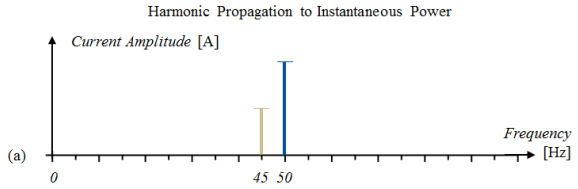

(a) A current with a oscillation mode (here 45 Hz, $2\phi/3$ phase shifted) is assumed for this example case. The voltages are not shown, but assumed to be completely sinusoidal at the fundamental frequency of 50 Hz.

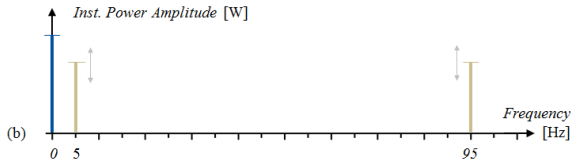

(b) The 45 Hz oscillation of the currents lead to either 5 Hz, or 95 Hz oscillation on the instantaneous power, depending on the sequence (positive or negative) of the current oscillation mode.

Figure 2.3: Example for the propagation of a current oscillation mode towards instantaneous real power oscillations.

reasons for instantaneous power oscillations. A combined analysis of the raw measurement data and the instantaneous real (and imaginary) power data is required to identify the origin of oscillation modes.

Application: Shunt Active Filter Shunt active filter handle the improvement of power quality in 3 phase systems. Depending on the nature of the network, different control algorithms are necessary to find the compensation currents, needed to improve the power quality. The shunt active filter focus on the mitigation of the harmonic content on the currents and will not address the compensation of large power oscillations. However, as the current oscillations lead to voltage drops along (e.g. line-)inductivities in the network, also small voltage oscillations will be mitigated. By implementing a control algorithm as in fig. 2.4 that compensates for imaginary- and oscillating real instantaneous power, the gating signals to shape the inserted currents are determined.

Following the discussion in the first chapters, some electrical systems will hardly be in a steady state but more continuously show transient behaviours throughout the whole operating time. Following this, also the compensation of harmonics need to be designed according to this behaviour. Classically, linear filters are used to split the average- ($\overline{p}$) from the oscillating instantaneous real power ($\tilde{p}$). The non-linear Empirical Mode Decomposition shows potential to be applied here instead.

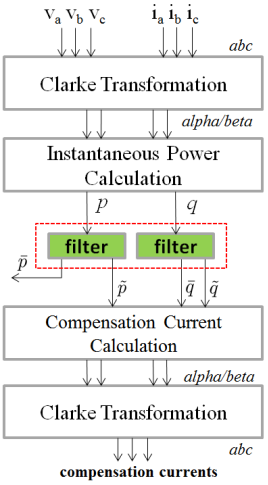

Figure 2.4: Flow chart of the control for a Shunt Active Filter. The compensation currents are calculated based on the instantaneous pwer-theory.

2.3.3 Norms on Measurement Equipment

Different norms can be found, describing measuring techniques and definitions of signal distortion. Mainly, the classical definition of power is used and measures like Total Harmonic Distortion or reactive power indicate the efficiency of a system.

- IEC 6100 Part 4-7 (2002): Testing and measurement techniques - General guide on harmonics and interharmonics measurements and instrumentation, for power supply systems and equipment connected thereto.
- IEC 61000 Part 4-30 (2015): Testing and measurement techniques - Power quality measurement methods.
- IEEE Std. 1459 (2010): Standard Definitions for the Measurement of Electric Power Quantities Under Sinusoidal, Nonsinusoidal, Balanced, or Unbalanced Conditions.
- IEEE Std. 519 (2014): Recommended Practice and Requirements for Harmonic Control in Electric Power Systems

However, as in networks with highly distorted fundamental ferquency, the power quality is assumed to be wrongly indicated by the suggested methods, as the Fourier transformation, as a key-player in the calculation of the classical measures shows disadvantages as discussed. Measurement equipment that is manufactured according to the norms is not necessarily giving true results on the system state. Some high-end devices have more possibilities to analyze the quality of voltage, current and inst. power of a network as suggested in the norms. However, detailed information about the calculation method of harmonic components are usually not given in data sheets of most manufacturers.

- Hioki has two devices PW3360 (Power Logger) and PW3390 (Power Analyzer). They don't refer to any standards for calculating power quality measures, and use classical power definition.

- Fluke-430 Three-Phase Power Quality and Energy Analyzer work according to IEC 61000-4-7 & -4-30. PLL implemented.

The Fluke-430 (as one example) shows possibilities to investigate the waveform and to detect electrical system dynamics. However, no device or norm was found that could rate the quality of a network, based on the analysis of fundamental frequency fluctuation.

2.4 Signal Analysis

Three phase networks are complex systems that can be analyzed either as three single phases or as a whole system with inherent properties. The three phases are defined by their voltage and current values respectively, named "raw measurements" in this thesis. This chapter focuses on detailed and very fundamental analysis methods of voltages, currents (single phase and system) and instantaneous power.

The instantaneous measured value of each voltage or current on a single phase can be represented as the real part of a complex vector $\overline{x}_t$, rotating at a certain frequency ω_t where the vector can be composed of components (modes) of different amplitude and frequency. Fig. 2.5 shows such a rotating vector. Equ. 2.12 and 2.13 show the mathematical description of the vector in sinusoidal and phasor form respectively.

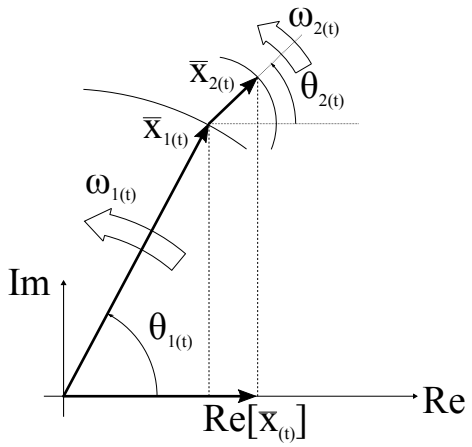

Figure 2.5: Representation of a single voltage or current vector with time-variant frequency and amplitude. Shown are the fundamental frequency- and one upper frequency component.

$$\overline{x}_{(t)} = \sum_{n=1}^{m} \left[amp_{n(t)} \cdot sin\left(\omega_{n(t)} t\right) + amp_{n(t)} \cdot cos\left(\omega_{n(t)} t\right) \right] \tag{2.12}$$

$$\overline{x}_{(t)} = \sum_{n=1}^{m} \left[amp_{n(t)} \cdot e^{j\omega_{n(t)} t} \right] \tag{2.13}$$

Here, $\overline{x}_{(t)}$ stands for the total komplex voltage vector, $amp_{n(t)}$ and $\omega_{n(t)}$ are the amplitude and frequency of the n^{th} component and m the total number of components.

Besides the fundamental component of the voltage or current, indicated by the subscript 1, also one higher frequency component (subscpript 2) is depicted in fig. 2.5. It could be assumed that the frequency and amplitude of the respective components are constant, but by doing so, two degrees of freedom are taken away and the resulting vector would only approximate the true vector. As soon as real measurement data is analyzed it is certain that all properties of the shown vector are non-stationary. Depending on the magnitude of variation, assumptions of steady frequency or amplitude might be justifiable. In some other cases the assumptions of constant properties lead to errors that exceed acceptable limits. Specially if the e.g. current- and voltage vectors are multiplied to obtain electrical power, deviations from the true value might increase.

As a physical measurement only records the real part of the vectors, it is a challenge to reverse-engineer information about the actual presence of all existing modes. In most cases only an approximation is possible and it has to be taken extensive care not to interpret the measurements in a wrong way. In some cases different combinations of vectors result in a similar real-part and reverse-engineering might lead to believe in the presence of vectors that can not be explained by any physical part of the network. Fig. 2.6 shows the measurements, taken in a ship-network during sea voyage besides clean sine-waves that are adjusted manually to fit the measurement as good as possible. These measurements are analyzed in detail in the later chapters of the thesis.

High frequency harmonic components (in the range of several kHz), originated by power electronic components are present in nearly every network nowadays. Besides power electronic components, other reasons for high frequency components might be electro magnetic interference, however, most likely with only neglectable small amplitudes . Low frequency modes or parameter variations might be present, but can not be observed in the short extract in fig. 2.6.

Positive-, Negative- and Zero Sequency Components: Three phase (3- and 4-wire) system measurements generally can be split up in three components. The positive sequence, which usually is responsible for most of the systems activity, a negative sequence which accounts for unbalance without the necessity of a neutral conductor and a zero-sequence that corresponds to voltage and current on the neutral conductor. A graphical representation of the three sequences is shown in fig. 2.7. Generally, 3-phase signals, either currents or voltages, might show harmonics at multiple of the fundamental frequency (indicated by integer subscript n). In

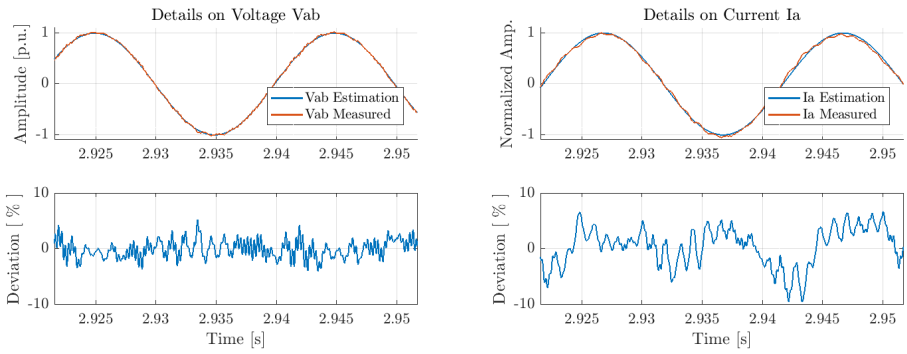

Figure 2.6: Measurements, taken on a network of a ship during sea voyage. The measurements are displayed beside a clean sine wave and the difference is shown. Respectively for line-voltage v_{ab} in the left figure and phase-current i_a on the right side.

this case, sequences can be found for each harmonic content separately. Equation 2.14 shows the mathematical calculation of the sequence components for a specific frequency-component of the signal [20].

$$\begin{bmatrix} X_{+n} \\ X_{-n} \\ X_{0n} \end{bmatrix} = \frac{1}{3} \begin{bmatrix} 1 & 1 & 1 \\ 1 & \alpha & \alpha^2 \\ 1 & \alpha^2 & \alpha \end{bmatrix} \begin{bmatrix} X_{an} \\ X_{bn} \\ X_{cn} \end{bmatrix} \tag{2.14}$$

X_{an}, X_{bn} and X_{cn} stands for the voltages or currents in abc-reference frame. α is a complex 120° phase shift operator.

The magnitude of the 3 phase voltages or currents in a sequence component (e.g. voltage phasors a, b and c in the positive sequence of the fundamental 50 Hz oscillation) are equal by definition and phase shifted by 120°. X_{+n}, X_{-n} and X_{0n} in fig. 2.7 represent the positive-, negative and zero sequence magnitude respectively, where X can be a voltage or current. Fourier transformation or a Phase Locked Loop (PLL) are the classical methods to extract the fundamental frequency, usually the one of most interest. The Empirical Mode Decomposition shows potential to be applied instead.

Transformation of Line- to Phase-Voltages: When measurements are taken, the setup is usually to record line-voltages V_{ab}, V_{bc} and V_{ca} and phase currents I_a, I_b and I_c. Thus phase-voltages (V_a, V_b and V_c) would require a physical neutral point (usually not available in a 3-phase, 3-wire system) and the line-voltages require to connect and measure simply the potential difference between the lines, the line-voltages are obtained in most cases. An advantage of line-voltage measurements is that only two line-voltages and phase-currents are needed to calculate a representation of the whole system.

The relation between phase-, and line-voltages is shown in equ. 2.15 to 2.17.

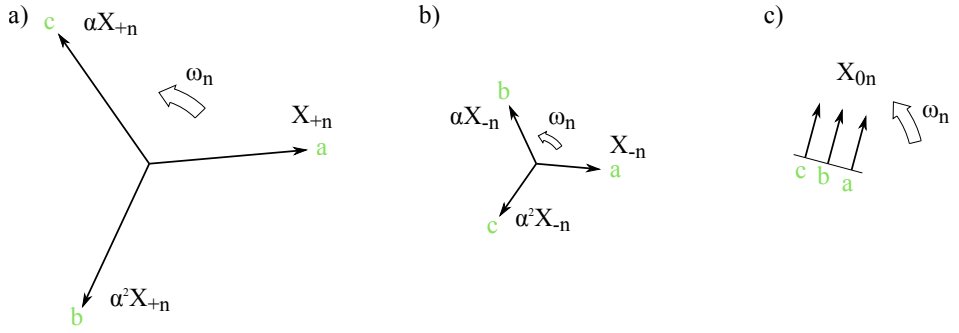

Figure 2.7: a) Positive-, b) Negative- and c) Zero-Sequences of a 3-phase, 4-wire network.

$$V_{ab} = V_a - V_b \tag{2.15}$$

$$V_{bc} = V_b - V_c \tag{2.16}$$

$$V_{ca} = V_c - V_a \tag{2.17}$$

In a 3-phase, 4-wire system, it is preferable to measure phase voltages, as they offer the possibility to consider neutral (zero-sequence) voltages. The line-voltages do not give any information on the unbalance of a system, and it is not possible to reconstruct the unbalance mathematically without taking assumption of the unbalance being evenly distributed on the phases, which might not be the case, or by making use of information on impedances and currents.

The calculation of phase-voltages from measured line-voltages can be done by means of equ. 2.18

$$\begin{bmatrix} V_a \\ V_b \\ V_c \end{bmatrix} = [M] \begin{bmatrix} V_{ab} \\ V_{bc} \\ V_{ca} \end{bmatrix} \tag{2.18}$$

with different possibilities for M. Within this Thesis the matrix from euq. 2.19 is used. A derivation and other possible matrices are discussed in appendix A. The variation between the phase-voltages obtained from different matrices M is marginally small, however it can be assumed that if the noise shows a governed frequency it can influence the performance of the non-linear Empirical Mode Decomposition method. Mode mixing problems might occur.

$$M = \begin{bmatrix} \frac{1}{3} & 0 & -\frac{1}{3} \\ -\frac{1}{3} & \frac{1}{3} & 0 \\ 0 & -\frac{1}{3} & \frac{1}{3} \end{bmatrix} \tag{2.19}$$

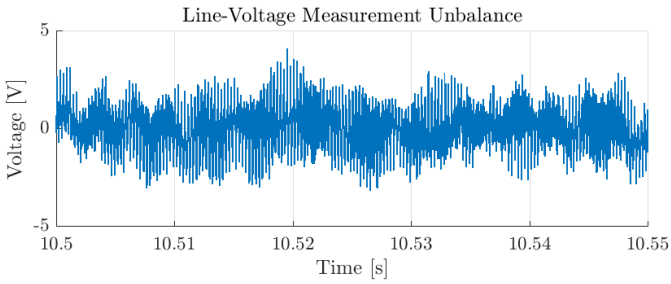

Figure 2.8: example case for unbalanced line-voltages

For balanced networks and flawless measurements, the matrices from the appendix result in the same phase voltages. However, as real measurements usually are susceptible to measurement errors it can be observed that line-voltage measurements show a unbalance (example from the ship-measurements shown in fig. 2.8). By their definition, line voltages are balanced, independent on the phase-voltages. If line-voltage measurements show unbalance, measurement errors must be assumed (Whatever 3 voltages there are, the sum of the phasors connecting them is always zero in theory).

2.4.1 The Empirical Mode Decomposition

The Empirical Mode Decomposition (EMD) is a a tool that aims to separate oscillating modes of different properties (most important property: frequency) into Intrinsic Mode Functions (IMFs).

The residue that can not be allocated to any of the IMFs, being a monotone signal is returned separately. The sum of all IMFs and the residue sums up to the original signal. The EMD is based on the algorithm shown in fig. 2.9.

Similar to the FFT, it shows great potential to separate signal of different frequencies from each other so that the analysis of the frequency bands can be done separately. In electrical systems, different physical components or mechanisms (electrical machines, converters, resonances, ...) leave prints of different properties on the voltage and current signal. The aim of any analysis should be to study the prints that can be allocated to a mechanism correctly. For strongly time-varying and non-linear signal, the FFT comes to its limits and the EMD, as a non-linear method, shows its advantages. If one mastered the tuning of the EMD successfully, it is a novel algorithm that has potential to replace the FFT in many applications within the control and analysis of electrical systems.

Focus lies on generating IMFs that represent the imprint of one (and only one) single physical mechanism (e.g. the inverter control to generate a fundamental voltage frequency, or the PWM of the power electronic switching). The IMFs usually are processed with the Hilbert Transform to obtain their instantaneous frequency and -amplitude. The whole analysis method, comprising EMD and Hilbert Transform is called Huang-Hilbert Transform (HHT) [6].

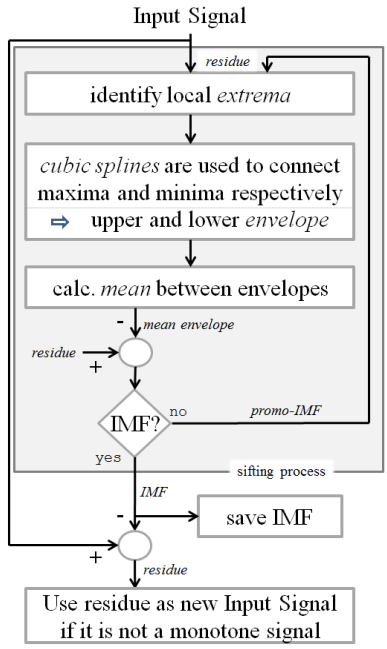

Figure 2.9: The algorithm of the Empirical Mode Decomposition

In some cases, the EMD is not capable of separating two modes from each other successfully. One reason might be that the time-varying frequency of two modes are approaching each other too close. Mode mixing is likely to occur. To overcome mode mixing, possible modifications of the original EMD exist. The basic EMD procedure has some *tuning* opportunities. The *tuning* pertains the sifting procedure. In fig. 2.9, the sifting stops, if IMF-criterion are fulfilled. In software implementations, the criterion are:

- All maxima must be positive and all minima negative
- The mean envelope can not exceed a certain error-value
- To limit computational afford, a max. number of sifts is defined.

Here, the first criterion can not be adjusted in any way. However, the second criterion, the error value of the mean envelop can be adjusted. It should be as small as possible and only allow computational errors, however, can be increased. The effect is, that the extracted IMF could contain a small amplitude, low frequency oscillation, which would become visible if the mean envelope is plotted. One more possibility to adjust the basic EMD procedure would be to multiply the promo-IMF (again, fig. 2.9) with a factor $a < 1$. More sifting iterations will be needed as the IMF is approached slower. The method compares to a *learning rate* in computer science [21].

Another way to overcome mode-mixing is the ensemble-EMD by Wu and Huang [22]. The basic idea is to add random white noise to the signal and perform the EMD-procedure. This is done several times. The actual IMFs are calculated by averaging between the IMFs of each EMD procedure. *"This new approach utilizes the full advantage of the statistical characteristics of white noise to perturb the signal in its true solution neighborhood, and to cancel itself out after serving its purpose"* [22]. With an high enough number of repetitions, the white noise cancels out and the sum of all IMFs plus the residue approaches the original signal with a negligible small error. The number of necessary repetitions depends on the signal.

Besides the ensamble-EMD, the mask-EMD by Deering and Kaiser [23] is another version to mitigate mode-mixing. If a frequency f_1 with a low amplitude is neighboured by an lower frequency f_2 with a high amplitude, it is likely to not be extracted in a separate IMF. The mask at the frequency of f_1 is added to the original signal and intends to highlight the maxima of the neglected signal. If separated successfully, the musk must be subtracted from the corresponding IMF again.

All together, the EMD, as a non-linear method needs to be adjusted to the signal. The more complex the signal is, the more empirical iterations and tuning approaches must be done to extract meaningful IMFs.

2.4.2 Clarke and Park Transformation

The signals obtained in a electrical three phase (3-wire or 4-wire) network can be either assessed as single phase signals (3 phases and evtl. neutral conductor) or as a representation of the whole network. Which method is more meaningful depends on the topology of the system and on the effects that are intended to be observed. If the phases are loaded independently of each other (e.g. loads, connected to a household socket), single phase analysis might be meaningful. If a load is connected to the three phases simultaneously (e.g. electrical machines or for DC transmission) it is more meaningful to investigate the signals in a different reference frame.

Clarke Transform The Clarke Transform projects the measurements from a 3-axis (abc) reference frame towards a 2-axis ($\alpha\beta$) reference frame as in fig. 2.10a. The values on the $\alpha\beta$-axis are oscillating at the fundamental frequency.

$$\begin{bmatrix} X_\alpha \\ X_\beta \end{bmatrix} = \sqrt{\frac{2}{3}} \begin{bmatrix} 1 & -\frac{1}{2} & -\frac{1}{2} \\ 0 & \frac{\sqrt{3}}{2} & -\frac{\sqrt{3}}{2} \end{bmatrix} \begin{bmatrix} X_a \\ X_b \\ X_c \end{bmatrix} \tag{2.20}$$

Park Transform The Park Transform projects the measurements from a 3-axis (abc) reference frame towards a rotating 2-axis (dq) reference frame as in fig. 2.10c. The rotation of the axis can be obtained by a Phase Locked Loop (PLL). In real life, e.g. in situation where the fundamental frequency is not constant 50 Hz, the PLL might not be able to follow the actual fundamental frequency exactly.

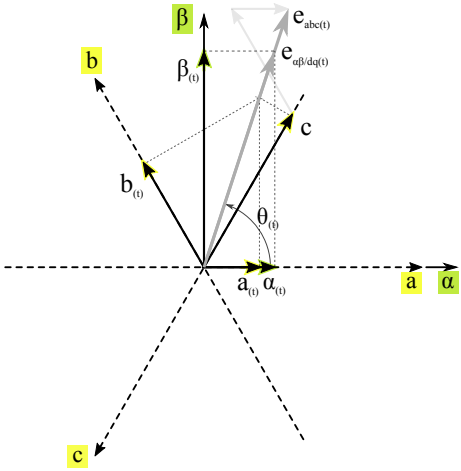

(a) Clarke Transformation. abc to $\alpha\beta$

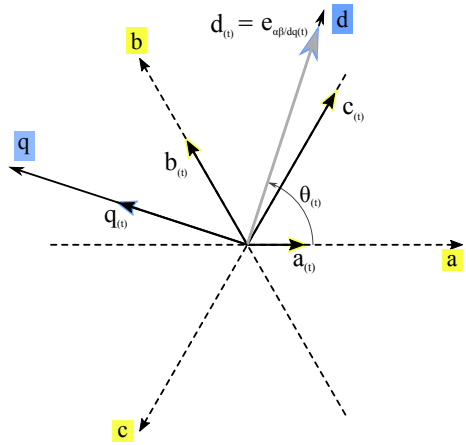

(b) Park Transformation. abc to dq

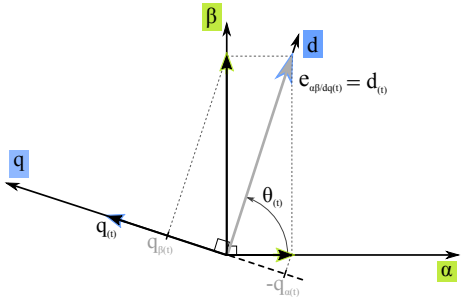

(c) Park Transformation. $\alpha\beta$ to dq

Figure 2.10: Transformation between reference systems for 3-phase voltages and currents.

$$\begin{bmatrix} X_d \\ X_q \end{bmatrix} = \sqrt{\frac{2}{3}} \begin{bmatrix} \cos(\theta) & \cos\left(\theta - \frac{2}{3}\pi\right) & \cos\left(\theta + \frac{2}{3}\pi\right) \\ -\sin(\theta) & -\sin\left(\theta - \frac{2}{3}\pi\right) & -\sin\left(\theta + \frac{2}{3}\pi\right) \end{bmatrix} \begin{bmatrix} X_a \\ X_b \\ X_c \end{bmatrix} \tag{2.21}$$

The 90 phase shifted d-, and q-axis correspond to the $\alpha\beta$ axis from the Clarke transformation, but rotate at the fundamental frequency (fig. 2.10c) so that the values on the d- and q-axis remain constant. Oscillations other than the fundamental frequency on the abc-axis will lead to oscillations (at a transformed frequency) on the dq-axis.

$$\begin{bmatrix} X_d \\ X_q \end{bmatrix} = \begin{bmatrix} \cos(\theta) & \sin(\theta) \\ -\sin(\theta) & \cos(\theta) \end{bmatrix} \begin{bmatrix} X_\alpha \\ X_\beta \end{bmatrix} \tag{2.22}$$

2.4.3 Estimator-Analyser of Power Quality

"Estimator-Analyser of Power Quality" is the name of a method or device, developed under the lead of Tomasz Tarasiuk from Gdynia Maritime University, Department of Ship Electrical Power Engineering [19, 24, 25]. It comprises the use of the Discrete Wavelet Transform (DWT), Fourier Transform and Chirp z-transform (CZT) where the evaluation method is chosen by previous evaluation of the input signal characters. The method aims to analyze non-stationary (most of it, variation in fundamental frequency) signal in electrical networks. This is, to overcome the challenge of correct window-sizing. The estimator-analyser of power quality therewith works on very similar tasks as the methods that are focused on in this thesis.

With the friendly support of Tomasz Tarasiuk, this thesis uses data that were recorded at Gdynia Maritime University.

Chapter 3

Methodology

The main aim of this thesis is to detect extensive variation of the fundamental frequency by means of a nonlinear analysis method - the EMD. Data, recorded on a maritime vessel serves as an example and the analysis is tailored to this system.

Many different signals are worth to be investigated in a electrical system. Most relevant however are investigations where the three phases are handled as a cohesive system and not as three separate single phase systems . In the physical level where the measurements that are taken, they appear as recordings of single phase quantities. Usually the phase-currents and line-voltages are recorded. This measurements need to be processed in order to obtain information about the 3-phase system. The total immediate power flow (instantaneous power) is a very useful quantity to be analyzed. Also the rotating voltage and current space vector can be obtained by suitable calculation based on Clarke transformation and reveals more information about the the voltage and currents of the system. In comparison to the instantaneous power, the vectors do not mix information from voltages and currents so that it is possible to detect details that are lost when the multiplication is conducted to obtain power.

The Hilbert Huang Transformation is the basic method to determine instantaneous frequencies of the modes in a signal, comprising of the EMD and a Hilbert Spectrum. The EMD is the core of the HHT to separate the modes and shows potential to be applied to multiple kinds of data in electrical systems. Raw measurements as well as post-processed signals can be analyzed with it. The analysis here will comprise the work with voltage- and current measurements as well as derived quantities like voltage and current rotating vectors and 3-phase instantaneous power. Each of those signals, measured and processed, can unveil effects that are hard to observe in the respective other one.

3.1 Investigate Voltages and Currents

For investigation of the voltages and currents, basically two methods can be used. The single phase measurements can be analyzed separately which reveals unique

information if single-phase loads are connected. On the other side, the three phases can be conducted to a rotating space vector so that information on the system behaviour can be investigated. In contrary to instantaneous power, information from voltages and currents are not buried by the multiplication of both.

3.1.1 Single Phase Voltages and Currents

As the provided measurements from the voyaging vessel are line-voltages and phase currents, these are analyzed as shown in fig. 3.1. During this analysis, first information from the signal is obtained and the tuning of the EMD needs to be adjusted to obtain meaningful IMFs. To avoid manipulation by transferring the line-voltages into phase-voltages, the original raw measurements are analyzed here.

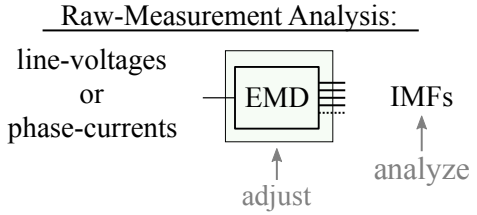

Figure 3.1: Initially, the raw single-phase measurements are analyzed. The EMD needs to be tuned to obtain meaningful results. As oscillatory signal without an offset is expected, the residue should be negligible small.

Sequence Analysis: Sequence analysis includes the separation into fundamental and harmonic components. Usually linear filters (or alternatively Fourier Analysis) are used to separate the fundamental oscillation from the harmonic content on the signal as done by Akagi in [20]. The attempt of the thesis is to renounce linear filters and the Fourier analysis.Non-liner filter methods like the EMD could be used instead of linear filters in order to extract the fundamental oscillation component of the measurement signal. Extending the scope of the thesis, the sequence analysis is suggested as further work.

3.1.2 Common Rotating Voltage and Current Space Vectors

A space vector, that includes all three voltage-, or current phases can be constructed as shown in fig. 3.2. The 120°phase shifted raw measurements are processed to α and β components with a Clarke transformation. Further on, the α and β components are used as real-, and imaginary components to construct a complex vector. This complex vector is referred to as "space vector" within this thesis. The magnitude of the space vector corresponds to the instantaneous amplitude. The time-derivation of the angle of the complex vector corresponds to the instantaneous frequency.

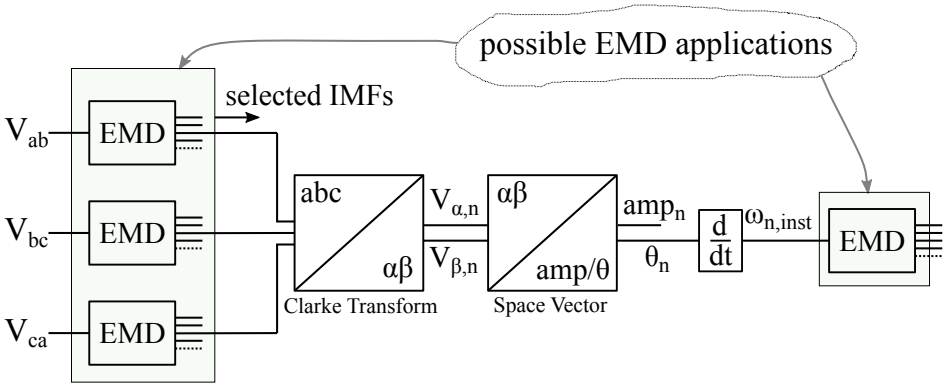

Figure 3.2: Procedure for analysing instantaneous frequency of the voltage space vector. For the current space vector the same steps are followed and the three phase-currents serve as input.

The EMD can be used at two different positions within this procedure. On one hand, the line-voltages can be split into IMFs, so that only certain modes are forwarded to the Clarke Transformation. For example, the 1^{st} IMFs of all three phases could be forwarded. The resulting space vectors will have constant amplitude if the three IMFs have the same frequency and are phase shifted by 120. Care must be taken that the IMFs from the 3 phases contain the same frequency mode.

On the other hand, the EMD can be applied to the instantaneous frequency. In that case, it should be known what to expect, because the Clarke transformation mixes all modes from all 3 phases together. The result might be complex to analyze. If there is too much noise coming up in the instantaneous frequency, the EMD could be used as a low-pass filter by neglecting high-frequency IMFs and summing up low-frequency IMFs and the residue. This would open the possibility to investigate slow variation of the fundamental frequency. Knowledge about the signal is crucial, to manually select the correct IMFs. By determining the instantaneous frequency of the IMFs, one has to be aware, that the frequency of the frequency-variation is investigated.

Fig. 3.3 shows the example case on what to expect from the space vector. Synthetic line-voltages are used.

3.1.3 Benchmark

As the application of the EMD on electrical network data has not been done before and no comparable trials are available, the resultand instantaneous frequency of the space vectors are compared against what is obtained by mature methods.

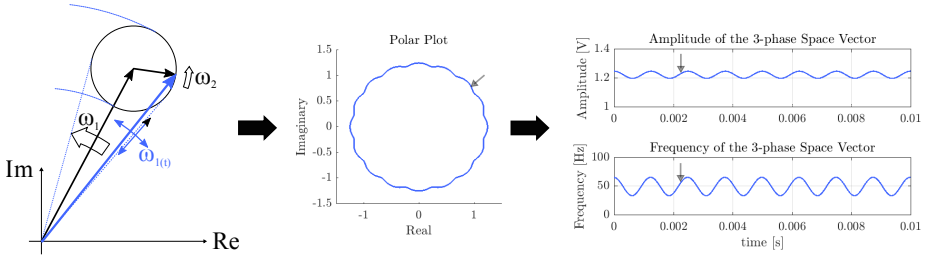

Figure 3.3: Example case for extracting instantaneous amplitude and frequency from a 3-phase space vector. The frequencies $\omega_1 = 50Hz$ and $\omega_2 = 850Hz$ as well as the amplitudes $a_1 = 1V$ and $a_2 = 0.02V$ are assumed constant here.

3.1.3.1 PLL

A PLL, developed by D'Arco et al. [26], is implemented in Matlab/Simulink and serves as a benchmark for the EMD-based instantaneous fundamental frequency analysis. The PLL is shown in Appendix B.

3.1.3.2 Mathematical average

A very simple low-pass filter is implemented by taking the mathematical average of a shifting time-window. This leads to a good approximation without phase-shift. The disadvantage of this method is that the first and last bit (half the window size) can not be analyzed and results are very rough. However, its simplicity is the main advantage.

3.2 Investigate Instantaneous Power

For the investigation of instantaneous power, the line-voltages can be transformed to phase-voltages. Instead of using the "2-Wattmeter"-Method, where only two line-voltages and phase-currents are necessary, the here proposed method evenly separates measuring errors onto the three phases and gives a more true average result. The "2-Wattmeter"-method would spread the measuring errors unevenly onto the phases. Fig. 3.4 shows the procedure, used for the analysis in this thesis. Here, it is only proposed to apply the EMD to the real and imaginary instantaneous power and not to the raw measurement data. At the current state of research, the IMFs, obtained from applying the EMD on the raw current and voltage measurements, are not expected to be clean enough to obtain meaningful instantaneous power from these modes.

A practical application of the method from fig. 3.4 is in the control of Active Shunt Filter, as shown in fig. 3.5. Classically, Butterworth filter are used to separate average from oscillating instantaneous real power. The oscillating part is supposed to be compensated by injecting compensation currents. A disadvantage of linear filters come to light when the system to which the Active Shunt Filter

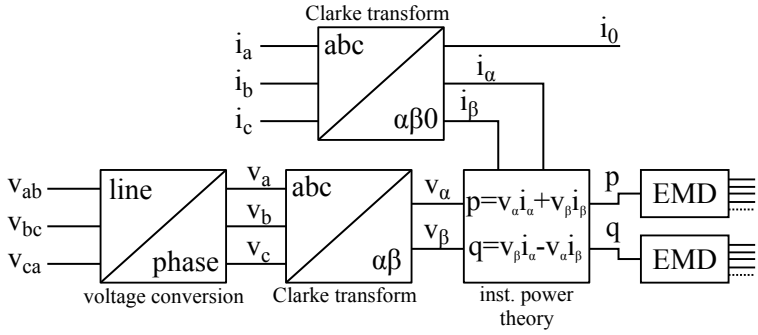

Figure 3.4: Procedure for analyzing instantaneous power.

is connected to, is in transient state. The delay that is an inherent property of the linear filter lead to time-delayed compensation currents and the power quality is worsened instead of improved. The application of the EMD does separate the components without an inherent delay. However, for real-time applications, a study of computational afford for the EMD needs to be conducted to check weather the procrastination through computational afford is small, compared to the inherent delay of linear filter.

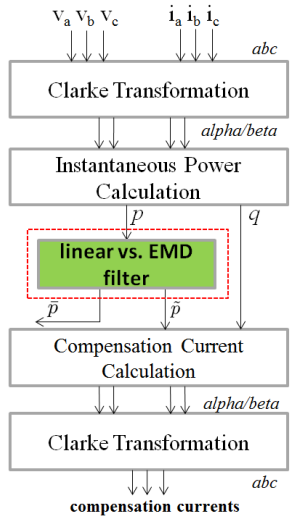

Figure 3.5: The EMD to separate oscillation modes in instantaneous power.

Chapter 4

Analysis

For the thesis, measurements, taken on a ship during sea voyage, are analyzed. This is mainly because no data from a 3-phase network in isolated rural environment is available in high enough quality. The measurements that were recorded by previous students onsite of Royal University of Bhutans student accomodation comprises information from a single-phase system and is therefore not suitable for the analysis in this thesis.

4.1 Comparability of Data

The situation on a ship is comparable in some means to the rural network in a developing country. The important property is a strongly variable load or supply that makes strong control action necessary to keep the frequency at the fundamental value. Power Electronic are used in both cases. In the rural network, usually within the converter that connects the DC generation unit to a AC grid. The ship uses power electronic converter to drive the gearless propulsion which comprises a back to back AC-DC-AC conversion where the network frequency is 50 Hz and the frequency of the propulsion depends on the wish for travel with the ship.

Measurements are from a vessel with electrical propulsion during 668.8 seconds of sea voyage. Three generation units (2x 425 kVA and 1x 200 kVa) and two azipods (gearless electrical propulsion) were active during the measurement. The sample rate is 30 kHz and a anti aliasing filter with a cut-off frequency of 10 kHz is used. Line voltages are recorded and compensated for offset and amplification factor for the voltage transducer and the anti-aliasing filter. The phase-currents at different locations in the network are recorded by means of Rogowski coils. Respective amplification factors have been applied. Positions in the network are at:

- Set 1: 200 kVA generator
- Set 2: 425 kVA generator
- Set 3: Propulsion drive (one of two)

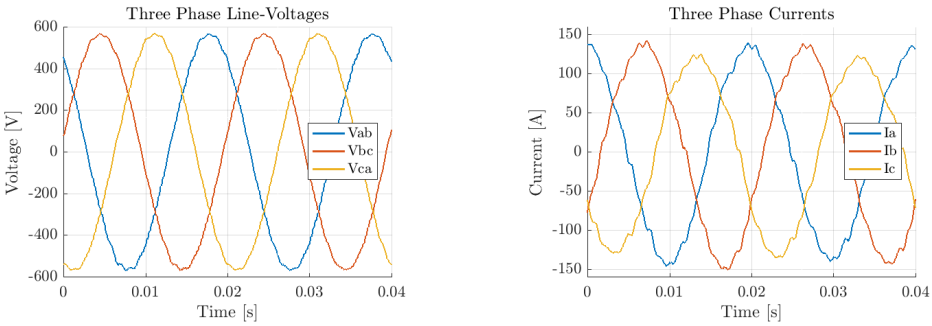

Figure 4.1: Extract of measurements recorded on a vessel with electrical propulsion during sea voyage. Left: Line voltages. Right: Phasae-Currents (Set 2), measured at the terminal of a 425 kVA generator

- Set 4: azimuth thruster drive (one of two)

4.2 Investigate Voltages and Currents

4.2.1 Single Phase Voltage and Current Analysis

The first analysis will be done on the raw measurement data, only compensated for measurement equipment-gain and -offset. These are the line-voltages and phase-currents which are shown in fig. 4.1. A 50 Hz sine-wave is clearly dominating the voltages and currents as expected from the system. The summation of voltages and currents respectively shows zero-sequence components in both cases. The zero sequence in the line-voltages do not show a dominating reoccurring behaviour, but oscillations at approximately 3-4 kHz and lead to the conclusion of measuring errors. The zero sequence of the phase-currents is shown in fig. 4.2. A dominant 50 Hz oscillation is present. To further investigate the voltage and current measurmentsl, the EMD is applied to separate different oscillation modes from each other. As it will be discovered within this chapter, the signal contains modes with time-varying amplitude and -frequency so that the tuning of the non-linear method must be adjusted to the properties of the measured quantities manually.

EMD on Line-Voltage Measurements: HF modes Applying the EMD on the line-voltage measurements, the resulting IMFs should represent modes at different frequencies. However, with the ship-measurements it turns out that broad mode mixing occurs at a variety of EMD-implementations and tunings. Finally, different implementations of the EMD need to be used to extract certain IMFs, so that the IMFs actually correspond to different frequency modes. The EMD that is used in a first trial to get an overview on the signal is EMD^1 (details see tab. 4.1). The 1^{st}, 2^{nd} and 3^{rd} IMFs of the three line-voltages are shown in fig. 4.3a, 4.3b and 4.3c respectively. Because mode-mixing occured in the high frequency

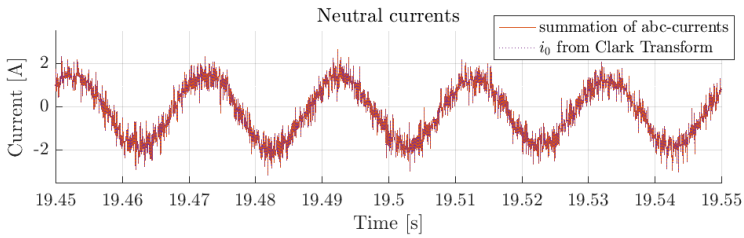

Figure 4.2: Calculation of neutral currents from the ship measurements Set 2. Method one: summation of phase currents. Method two: i_0 from Clarke Transform, handled with the factor of $\sqrt{3}$. The maximal error between the two methods is $1.8 \cdot 10^{-13}$ and can be neglected.

IMFs, the fundamental frequency is not separated in a single IMF, but is spread out in the IMFs 4-10 and the residue. These components are summed up and Fig. 4.3d shows the resultant signal, containing the fundamental frequency. For better visibility, only an extraction of 0.05 s is plotted.

The voltage signal appears to be very similar between the three phases. All IMFs coincide pretty well at a first look. However, differences come to light once they are analyzed in detail.

The observation of the first two IMFs shows amplitude oscillations with a period of 23.3 s, simultaneous on all three line voltages. By zooming into IMF 1, as in fig. 4.4, high-freuquency oscillation becomes visible. The frequency of the oscillation will be investigated with a Hilbert Spectrum in fig 4.6 later on, but another detail arises. The high frequency modes of the line-voltages oscillate against each other in pairs of two while the third line-voltage has a temporarily deceasing magnitude. After 0.01 s (100 Hz) the procedure repeats. An explanation for this behaviour would need more knowledge about the the ship system. Imaginary power, oscillating between the lines or effects, caused by converter control can be assumed.

In fig. 4.5, a zoom into only the 1^{st} IMF of V_{ab} is shown. A repetitive pattern in a period of 0.02s (50 Hz) can be recognized. Similar patterns are present at V_{bc} and V_{ca} (not shown separately).

Further investigations of the first IMF with the Hilbert method reveals the instantaneous frequency and amplitude. The Hilbert spectrum of a 120 s clip of the 1^{st} IMF of V_{ab} is shown in fig. 4.6 . Compared with the IMF by itself, the Hilbert spectrum confirms the amplitude oscillation (dark red color) at a low frequency of approximately 23.3 s as identified in fig. 4.3a already. Other than that no conclusions can be drawn by this figure as the frequency wildly fluctuates between 0 Hz and 14 kHz.

Further on, two time-instances will be analyzed in detail. The first instance, at 76.59 s (high amplitude), the second one at 87.42 s (low amplitude). Fig. 4.7a shows the first instance, where a swelling oscillation at a frequency of approximately 3.6 kHz is observed. Where the amplitude of the 3.6 kHz oscillation in fig. Fig. 4.7a is low, a higher frequency mode becomes visible, oscillating at a frequency of

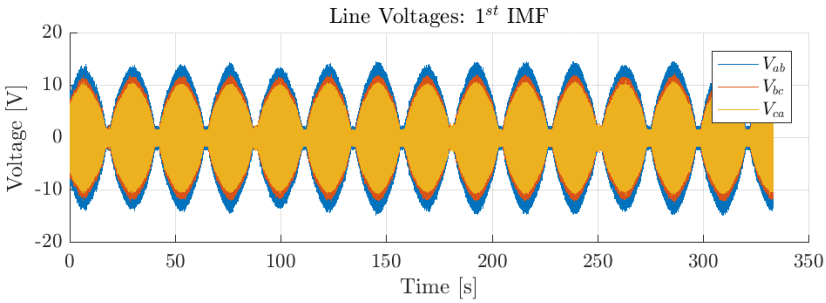

(a) Periodic amplitude swelling at a period of 23.3s. IMF 1 contains 7.5 kHz and 3.5 kHz modes

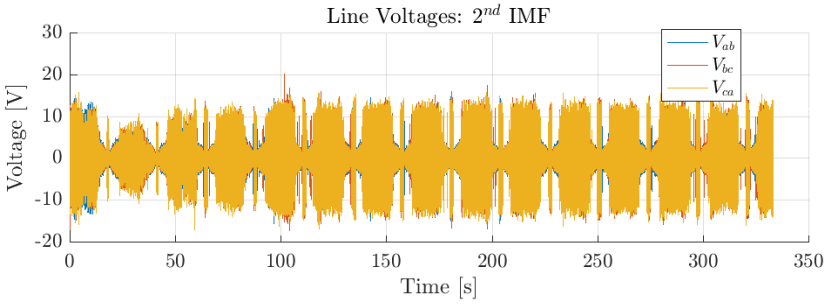

(b) Again periodic amplitude swelling. Amplitude also follows current trends. Strong mode mixing between 3.5 kHz and 850 Hz.

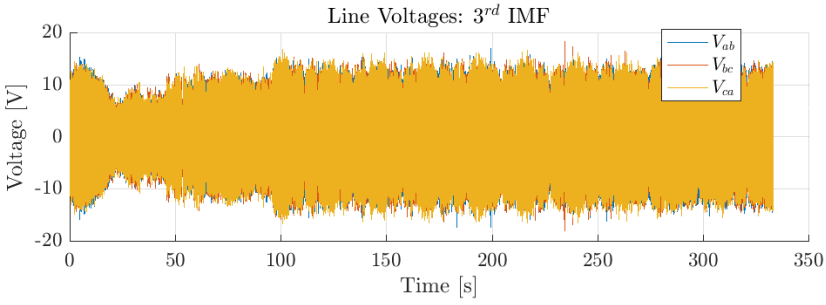

(c) Amplitude follows current trends. Mode mainly at 850 Hz and partly 560 Hz.

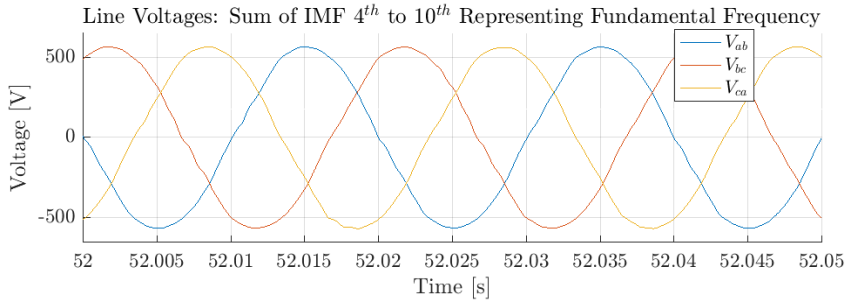

(d) The fundamental frequency modes. Sum of IMF 4 to 10 plus the residue. Also includes a mode at 560 Hz.

Figure 4.3: IMFs from EMD on line-voltages. 500 sifts and max. 10 IMFs + residue

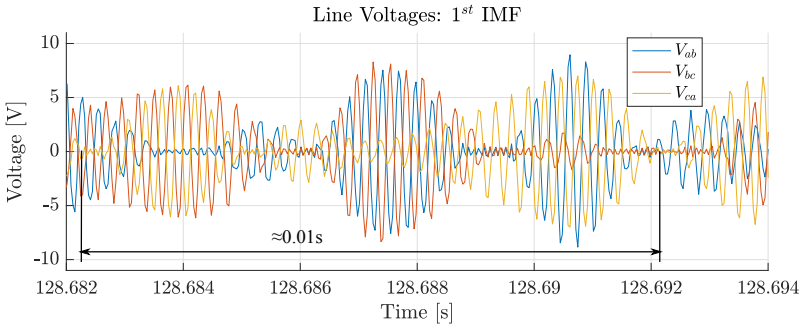

Figure 4.4: Extraction of 11.3 ms from fig. 4.3a - high frequency oscillation becomes visible. Two line-voltages are oscillating against each other while the third one has a deceasing amplitude. After roughly 0.01s recouring patterns can be interpreted.

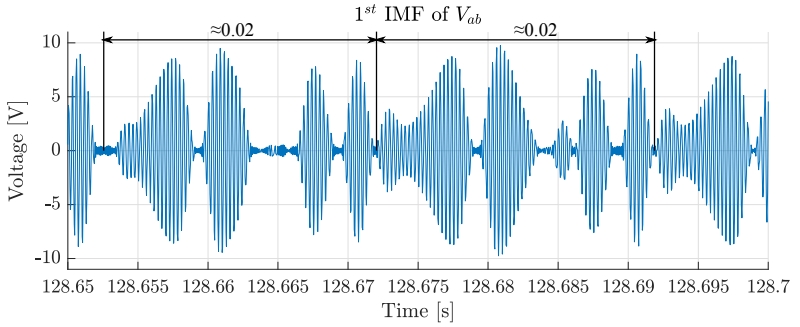

Figure 4.5: The first IMF of V_{ab} only. A repetitive pattern with a period of 0.02s in average is recognized.

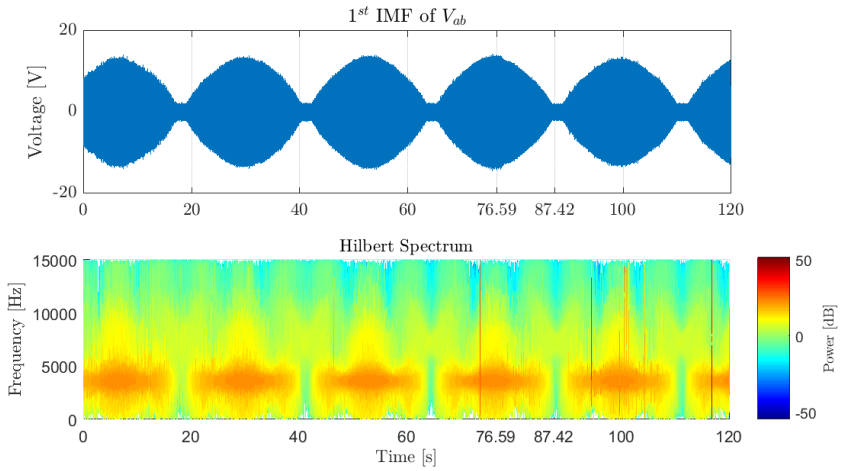

Figure 4.6: Analysis of the 1^{st} IMF of V_{ab}. Upper: The IMF. Lower: The Hilbert Spectrum of the IMF showing instantaneous frequency and amplitude

7.5 kHz approximately. It has to be recalled, that the anti-aliasing filter has a cut-off frequency of 10 kHz and the sample rate is at 30 kHz. Therefore, the resolution of high-frequency mode is doubtful as one period contains only 4 samples.

Fig. 4.7b shows the second instance where only the frequency mode at 7.5 kHz is visible.

The question arises why mode mixing occurs in IMF 1. Rilling et al. [27] gives answer to this question. With two modes of relatively close frequency and a low amplitude of the high frequency mode, the EMD is not able to separate the two modes. IMF 1 of V_{ab} (similar to V_{bc} and V_{ca}) shows two modes at a frequency ration of approximately $f = \frac{3.6kHz}{7.5kHz} = 0.48$. According to [27], in that case mode mixing is predicted to occur at a amplitude ratio of $log_{10}(0.4)$. As the amplitude of the 3.6 kHz mode varies from 14 V to 0 V, and the 7.5 kHz mode shows amplitudes around 2 Hz, mode mixing is explained by the theory at several instances. Rilling et al. did not investigate swelling-, but only stationary amplitude so that their results can indicate a reason for mode mixing but do not proof the reason for the observed mode mixing in the ship measurements. How their theory applies to swelling amplitudes needs to be investigated, however that exceeds the scope of this thesis.

Tuning of the EMD for the line-voltages: As explored, each of the line-voltage measurements shows a mode at approximately 7.5 kHz. This is very close to the sampling frequency of 30 kHz so that one period is defined by only 4 samples and no good resolution of the waveform can be expected. According to Nyquist and Shannon, an appropriate sample rate should be higher than ten times the

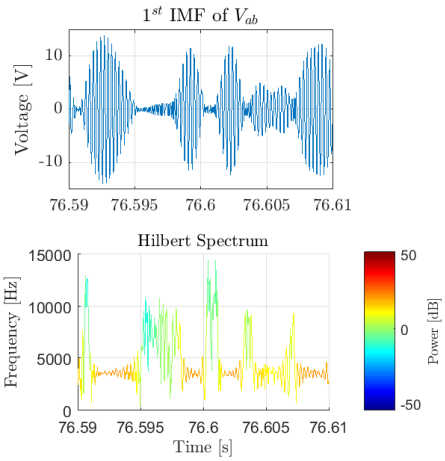

(a) T = 76.59 s, a swelling mode at approximately 3.6 kHz is identified. It explains the amplitude patterns observed in fig. 4.6.

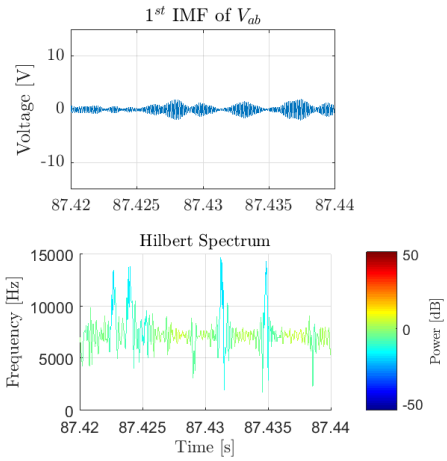

(b) T = 87.42 s the only mode present shows a frequency of approximately 7.5 kHz in the Hilbert Spectrum.

Figure 4.7: Details of IMF1 from V_{ab} generated by EMD with settings shown in table 4.1.

highest expected frequency. As the EMD depends on a good resolution to find the position of the extrema to precisely model the envelops, it is decided to use a mathematical average filter to remove the 7.5 kHz component from the signal, prior to applying the EMD. A window size of 4 samples, corresponding to 7.5 kHz is chosen. Further on, as a result from the trial EMD applications on different time-spots, two modes at 850 Hz and 560 Hz respectively were observed on V_{ab} and V_{bc}. V_{ca} showed only minor appearance of the 560 Hz mode while the 850 Hz mode is comparable to the ofther two line voltages. It can be assumed, that the 560 Hz oscillation is mainly only present on phase voltage V_b. Mode mixing is observed between all neighbouring modes in the IMFs from EMD^1. As a solution to achieve a good separation, the procedure, EMD^3 shown in fig. 4.8, is applied to extract the modes from V_{ab} and V_{bc}. For V_{ca}, consisting only of three major modes (3.5 kHz, 850 Hz, 50 Hz) after removing the 7.5 kHz noise, EMD^2 is applied directly.

EMD^3 can be describe as following. For each line-voltage, the noise of 7.5 kHz is extracted and a EMD^2 is applied to extract the first two IMFs. The remaining signal (*PRE-residue*) is added to a mask signal to prevent mode-mixing between the 560 Hz and the 50 Hz mode in the next EMD. The mask signal is again subtracted and the final IMFs obtained. As the voltages oscillate around zero, no residue is expected. In reality the residue shows negligible small activity with amplitudes of $1.5e^{-13}$ V. The wide-awakens of the method is to add the mask signal after the second IMF is extracted to emphasize the 560 Hz oscillation and guarantee extrema, which are important for the EMD to separate modes. Would the mask signal be added to the original signal, it would "melt" the 2^{nd} and 3^{rd}

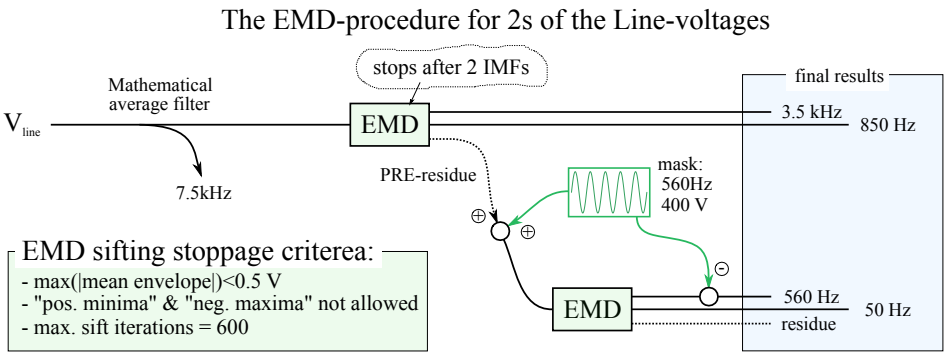

Figure 4.8: EMD^3: The procedure to separate the line-voltages measurements into IMFs.

signal together. Important is, that the mask is subtracted from the 3rd IMF, so the sum of all IMFs are equal to the original signal. The resultant IMFs for V_{ab} are shown in fig. 4.9.

The vast time-varying properties of the signal and a high computational afford of EMD^3 made it impossible to succeed in separating modes for the whole of the 668 s of measurement. However, compared to EMD^1 (fig. 4.3) where it is not possible to recognize the modes of the line-voltage signal, the improved procedure brings light into the actual mode-mess of the signal. Summarized, the signal contains noise at 7.5 kHz, high frequency modes at 3.6 kHz, 850 Hz and 560 Hz and the fundamental frequency mode at 50 Hz.

A research for open access EMD codes unveiled the code from Manuel Ortigueira, which is based on a paper from R.T. Rato et al. [28]. It is referred to as EMD^4. The tuning options are implemented with three factors. At first, *qResol*, which has an impact on the stoppage critereon for the sifting process. The value (recommended between 40 to 60) is interpreted as a ratio in dB and accounts for the energy of the mean envelop. It has an impact on the number of IMFs that the signal will be spread into. The second tuning parameter *qResid* (also in dB and recommended to be between 40 to 60) influences the definition of the residue. The last tuning parameter, *qAlfa* can be understood as some kind of learning rate. During the sifting process, after each sift, the resultant "promo-IMF" are multiplied by this factor. It usually is below 1. It was tried to apply the EMD to the ship-measurements, but not satisfactory tuning could be found.

EMD on Phase-Current Measurements: HF modes As done for the line-voltages, also the phase-currents are analyzed. For the sake of overview in the document, the results are not plotted and only set 2 (currents at the terminal of the 425 kVA generator) is treated. The dominant frequency modes are identified at 7.5 kHz, 3.6 kHz, and 50 Hz. One or multiple modes can be observed between approximately 500-1200 Hz with big mode-mixing issues. IMF 1 on all phases also shows activity that leads to the assumption that a mode at even higher frequency

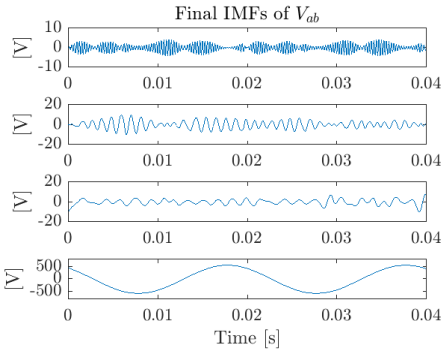

(a) The 4 IMFs from V_{ab}, shown on separate axis. The EMD procedure of fig. 4.8 is used to filter noise and prevent mode-mixing The residue is const. zero (not shown).

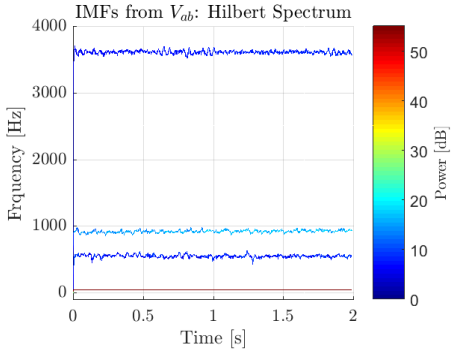

(b) The Hilbert Spectrum (median filter length = 500 samples). The fundamental frequ. of 50 Hz hides at the bottom of the graph.

Figure 4.9: The resultant IMFs and Hilbert Spectrum from line-voltage V_{ab}.

Table 4.1: Settings of the EMD to extract certain IMFs from line-voltage ship-measurements

	Description	credits
EMD^1	fixed number of sifts (500) and max. 10 IMFs	Geir Kulia
EMD^2	sifting stoppage criteria: - $max(\|meanEnvelope\|) < 0.5V$ - pos. minima and neg. maxima not allowed - max. sift iterations = 600	Geir Kulia
EMD^3	procedure explained in fig. 4.8	Geir Kulia
EMD^4	rParabEmd	R.T. Rato et al. [28]

(10-15 kHz) must be present, but as the sample frequency doesn't support good resolution on that high frequency, no statement on this mode can be done. Also, during several seconds all over the signal, a mode at 30-45 Hz can be observed on all three phase-currents. This mode does not occur simultaneously at the three phases, but it shows similar properties when it appears. More information on the network of the ship is needed to judge if this mode is made up by the EMD or if actually some low-frequency (below the fundamental frequency) mode is present on the signal.

4.2.2 Common Voltage and Current Space Vectors

After analyzing the line-voltage and phase-current measurements for each phase separately, the space vectors of voltages and currents are generated to obtain a statement on the system. As will be shown in the following paragraphs, it can be assumed, that not all loads consume their power from the three phases simultaneously, but that single phase loads are connected, too. The single phase loading, but also other effects will distort the results and lead to non-circular polar plots of the space vectors. At first, fig. 4.10 and 4.11 show the voltage and current space vectors, their amplitudes and angular speeds for the whole of the available data. Later on, and for the reason of computational afford, only fractions of the whole data will be analyzed. However, the first two figures reveal already known amplitude and frequency oscillation modes at a period of 23.3 s, reasoned by the 7.5 kHz oscillations. Further on, the amplitude of the current space vector gives information on the power consumption of the ship. Rising throughout the first minute, the consumption is stationary for most of the time and drops again for the last two minutes.

Based on the findings in the previous chapters, fig. 4.12 shows polar plots, generated of the IMFs obtained from each line-voltage by applying EMD^1. 80 s are shown. Only the polar plot of the fundamental frequency IMFs shows a circular shape because the time-course of the fundamental voltage oscillation is 120 degrees phase shifted and the amplitude of the space vector becomes nearly constant. IMF 1 and 3 (fig. 4.12a and 4.12b) of the line-voltages on the other hand show oscillatory behaviour as depicted in fig. 4.4. The space vector flips 180 degrees whenever two phases oscillate in opposite of each other. This is indicated by the black arrows. IMF 2 contains too much mode mixing to obtain any valuable information. As the amplitude of the high frequency oscillation is far smaller than the one of the fundamental frequency, fig. 4.12e shows all space vector graphs in one plot to better perceive their dimensions.

Further on, and to keep track of the main goal of the thesis, the fundamental frequency is analyzed. The two possible EMD-applications, discussed in the methodology chapter (fig. 3.2) are tried out on the ship data.

At first the results from EMD^1 on the line-voltages are handed into the procedure to calculate space vectors for each of the IMFs. That means, that the fundamental IMFs from V_{ab}, V_{bc} and V_{ca} are transferred to the $\alpha\beta$-reference frames and further used to built a complex "space" vector. The derivation of the angle

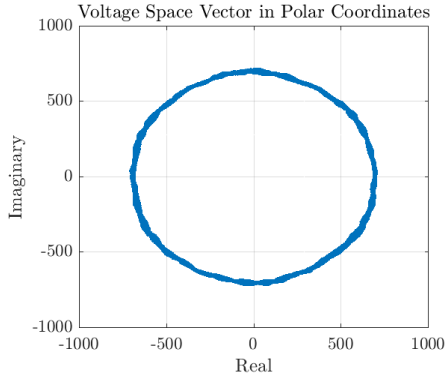

(a) The space vector in polar coordinates.

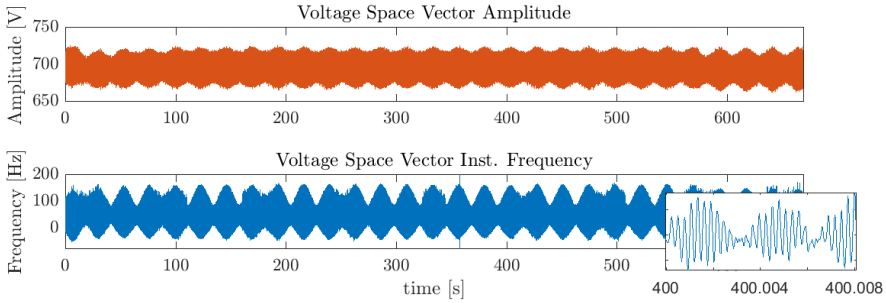

(b) Amplitude and angular speed. The amplitude variation at a period of 23.3 s from the 7.5 kHz mode is reflected in both, amplitude and angular speed.

Figure 4.10: 3-phase Voltage-Space-Vector from raw measurements.

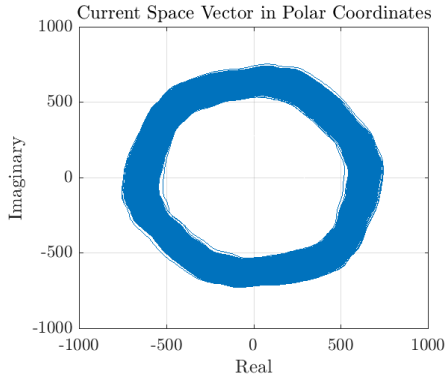

(a) The space vector from t = 100s to 550 s, to show the duration of approximately stationary amplitude.

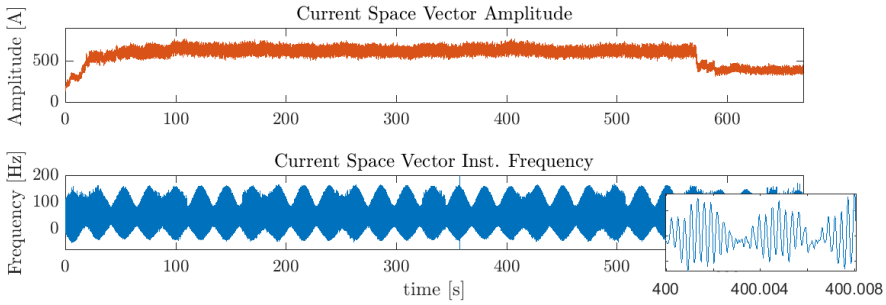

(b) Amplitude and angular speed. Noticeable is the amplitude graph that represents power consumption.

Figure 4.11: 3-phase Current-Space-Vector from raw measurements.

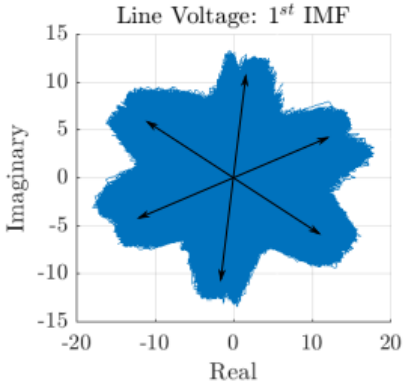

(a) Mode at 3.5 kHz

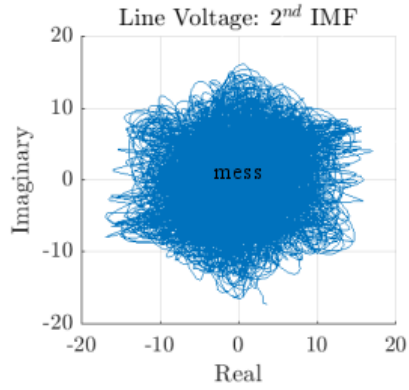

(b) Mode mixing between 3.5 kHz and 850 Hz

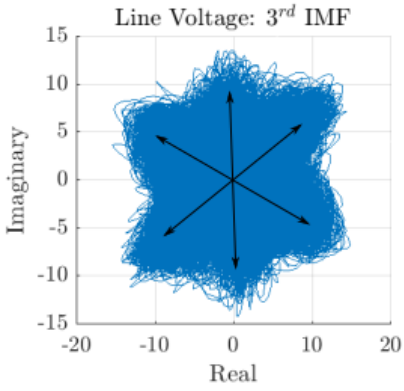

(c) Mode at 850 Hz

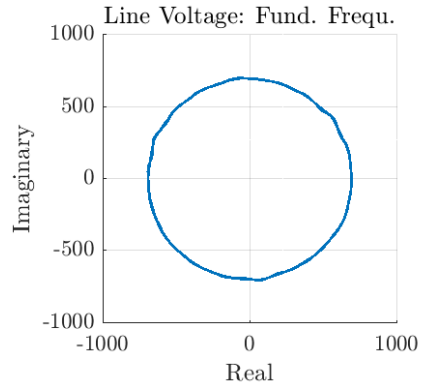

(d) Fundamental oscillation at 50 Hz + mode mixing with 560 Hz mode

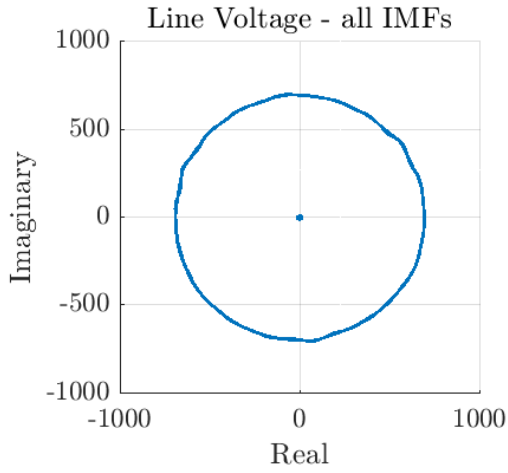

(e) For comparison of their dimensions, the grphs from a) to d) are shown on the same axis.

Figure 4.12: Plot of the space vectors being constructed by Intrinsic Mode Functions from line-voltages from all 3 phases respectively. EMD^1 is used.

gives the instantaneous frequency. As only the IMFs, containing the fundamental frequencies are processed, the resultant frequency of the space vector should be relatively smooth in theory. However, known from previous analysis, mode-mixing occurred and EMD^1 does not separate the modes perfectly. Instead, a noisy signal is obtained.

The second approach is to use the raw line-voltage measurements. The resultant instantaneous frequency of the space vector is expected to be highly polluted. However, from former analysis, certain frequency modes can be excluded from the signal as they are known to not belong to the fundamental frequency (3.5 kHz, 850 Hz, 560 Hz). The instantaneous frequency from the raw line-voltage measurements is shown in fig. 4.10b previously. The instantaneous frequency fluctuates from negative values up to nearly 200 Hz.

One weakness of the EMD is, that modes are expected to oscillatory. For the instantaneous frequency, that must not be the case. As stated in the research-chapter, the instantaneous frequency depends on the balance of generated- and supplied power. The power production of a PV-panel however would not follow a oscillating behaviour, but would occur randomly, depending on clouds, temperature and so on. In the ship, there is no information on power consumption/generation trends available. A good approach to use the results from the EMD on the instantaneous frequency is therefore, to sum the residue plus a certain number of low-frequency IMFs. The number of the low-frequency IMFs strongly depends on the nature of the signal and so far must be done manually and by ones perception.

Fig. 4.13 shows cases in wich the residue is summed to different selctions of low-frequency IMFs. In the next section, these results will be compared to what has been obtained with a PLL.

4.2.3 Benchmark

To compare the results from the previous chapter, the PLL from appendix B is used to extract the instantaneous fundamental frequency from the line-voltages. The result is shown in fig. 4.14, together with the closest solution obtained from the EMD. Also the results from a mathematical average calculation on the instantaneous frequency of the space vector is shown. It can be noticed, that the results from PLL and mathematical average coincide good, and the EMD mostly shows similar results, but differs for short periods as e.g. between 15 s to 20 s.

The same procedure as for the line-voltages was used to find the instantaneous frequency of the space vector, constructed from the phase currents. Similar results are found and the resulting instantaneous frequency, shown in fig. 4.15 is obtained by summing the residue and the last four IMFs together. As done for the voltages, also the PLL and a mathematical average calculation was applied, so that the EMD can be compared to the mature methods. For the line-voltages, both methods showed similar instantaneous frequency, but for the currents, the results differ quite strong. It is assumed that mode mixing in the high frequency IMFs is the reason for the big fluctuating fundamental frequency from the EMD-method.

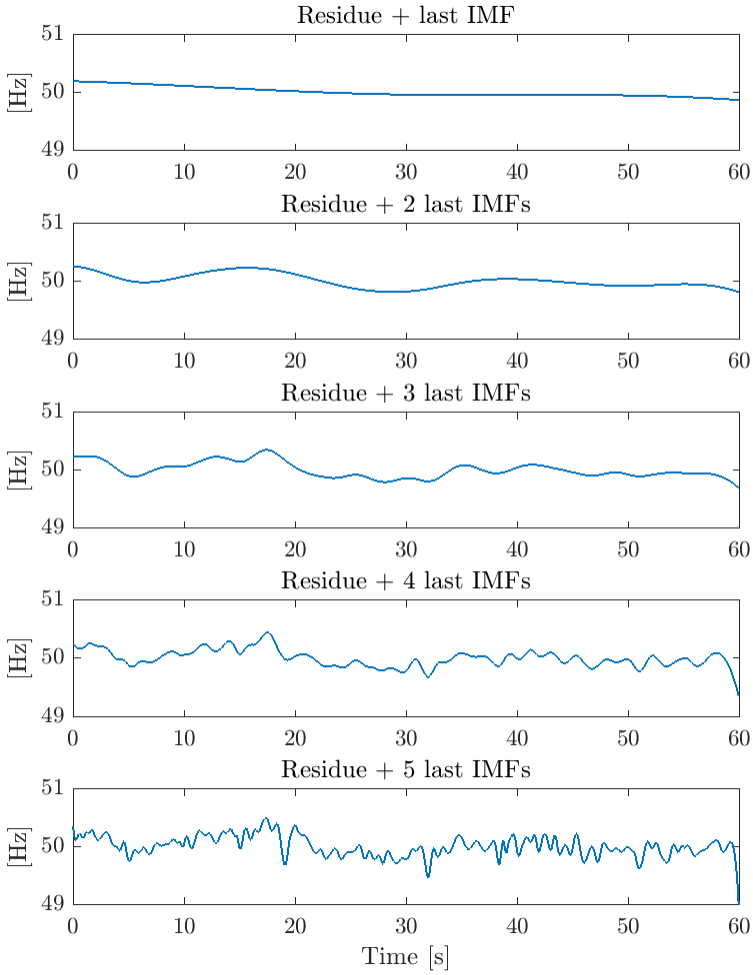

Figure 4.13: Reconstructing the instantaneous frequency of the voltage space vector (line voltages, 7.5 kHz filtered out). Gradually, low frequency IMFs from EMD^1 are summed to the residue.

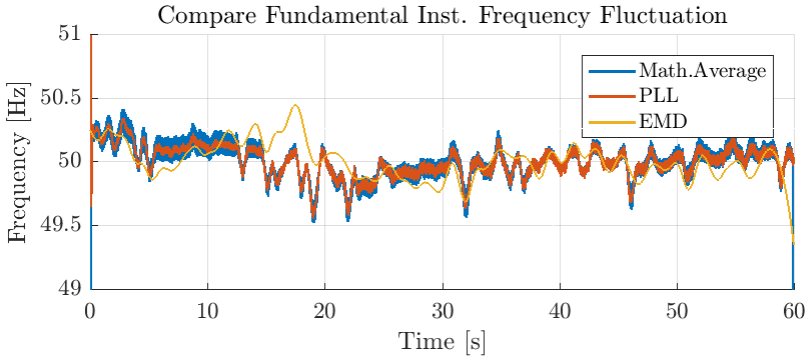

Figure 4.14: Voltage instantaneous fundamental frequency. Blue: The mathematical average (window: 3000 samples). Red: Results from the PLL (appendix B). Yellow: the four last IMFs plus the residue from EMD^1 applied to the instantaneous frequency of the space vector, calculated from line-voltages.

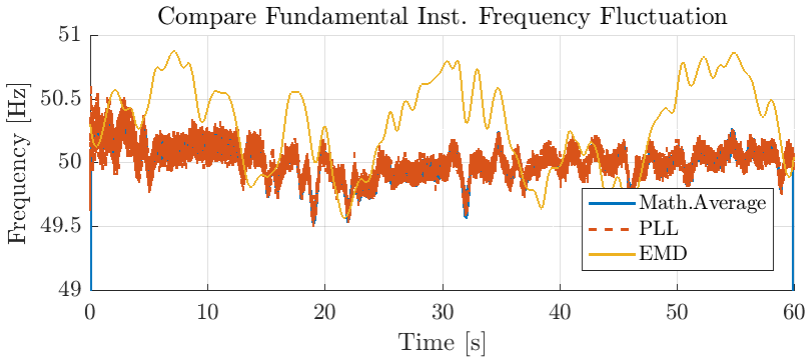

Figure 4.15: Current instantaneous fundamental frequency. Blue: The mathematical average (window: 3000 samples). Red: Results from the PLL (appendix B). Yellow: the four last IMFs plus the residue from EMD^1 applied to the instantaneous frequency of the space vector, calculated from phase-currents.

Figure 4.16: Instantaneous real- and imaginary power, measured at the terminal of the 425 kVA generator.

4.3 Investigate Instantaneous Power

The calculation of instantaneous power is conducted by means of the procedure shown in fig. 3.4. The currents from set 2 (terminal of the 425 kVA generator) are used for this example case. The resultant instantaneous real- and imaginary power is shown in fig. 4.16. To get an insight into the oscillation modes, the EMD is applied to the instantaneous real power graph. It reveals oscillation modes at 15 kHz, 7.5 kHz, 3.6 kHz, 1 kHz, 625 Hz, 300 Hz, 120 Hz and several slower modes without a governing frequency. All modes are fluctuating widely. The mentioned frequencies can be used as rough indicators only. Some modes are present only during certain time periods and mode-mixing makes it difficult to analyze the EMD-results.

The results from the EMD on imaginary power reveals similar modes. They are at the same frequencies approximately. Only the modes below 120 Hz and the residue differ significantly.

So far, only short time periods of the instantaneous power have been analyzed. The evaluation of longer periods is necessary to obtain information on low-frequency power oscillations. This needs to be done and is listed among the subsequent work for the thesis.

Application in Shunt Active Filter: A conference paper is written and focuses on the application of the EMD as part of the control of shunt active filter. The paper (title: "Impact of Time Varying Angular Frequency on the Separation of Instantaneous Power Components in Stand-alone Power Systems"), to be presented at the 6^{th} International Conference on Clean Electrical Power (ICCEP - 2017) benefits from the fundamental research conducted within this Thesis.

Chapter 5

Conclusion and Further Work

The main aim of this thesis is to analyze non-stationary fundamental frequency and to prove its existence in remote power grids. The Empirical Mode Decomposition is used as the key element for non-linear data processing. Based on the EMD, methods are developed and tested on signal, obtained from the 3-phase power system of a marine vessel.

Before starting with the analysis of the fundamental frequency, it is decided on three steps to gradually obtain an insight to the signal. First, the single phase voltage and current measurements are investigated. At a second step, complex space vectors are generated from the 3-phase voltage and current measurements respectively. Finally, the instantaneous power is calculated. From the first to the third step, the information from the raw-measurements are gradually mixed. Each stage offers information that is not possible to obtain on the others.

In the first step, the line-voltages and phase-currents are separated into Intrinsic Mode Functions and the instantaneous frequency of these modes is determined. By using a mask signal and a tailored tuning of the EMD, meaningful results are obtained. The converter switching frequency of 3.6 kHz, and several high frequency modes and the fundamental frequency are extracted from each other. In the second step, the instantaneous amplitude and frequency of the rotating space vectors are calculated. The EMD shows two possible application in the process. Either on the raw measurements so that space vectors for each mode result, or on the final results. The EMD is applied on the final results and, as a important result within the thesis, the fundamental frequency is constructed by summing up low frequency IMFs and the residue. Compared to mature methods (PLL and mathematical average), a conceptual prove for the possibility of the EMD to extract the fundamental frequency from a strongly distorted 3-phase signal is supplied. The performance of the EMD however, must be improved to to increase the quality of the signal. In the last step, the EMD is applied to instantaneous power. As all information from the 6 measurement channels are mixed together, the resulting signal is highly distorted. Mode mixing is again deteriorating the results from the EMD.

It can be noticed, that by conducting from the analysis of the raw measurements

to the investigation of instantaneous power, the performance of the EMD becomes more and more essential. The main priorities in the thesis are laid on explaining the theory behind 3-phase power systems, improving the performance of the EMD and concluding to statements on the electrical network from findings at the three investigation stages.

Further Work: Electrical networks show nearly infinite possibilities for novel investigations. The thesis covered the trial application of the EMD to extract non-linear and non-stationary signals. The biggest need to improve the work is to strengthen the capability of the EMD to separate complex signals including swelling amplitudes and modes at very close frequencies, without mode-mixing. It is needed to study the literature and to adjust the algorithm to the nature of the data. Once, the quality of the IMFs improve, more accurate statements on the investigated network will be possible. For further analysis of the data from the marine vessel, information on the network topology will lead to a better understanding of the findings. This information needs to be requested from Tomasz Tarasiuk from Gdynia Maritime University, where the measurements were recorded. Also, and as an interesting test of the capabilities of the EMD in comparison to the Fourier Transform, measurement data during maneuvering and not only sea voyage, could be requested. The fundamental frequency is expected to vary much stronger during maneuvering. Back to the origin of the idea for the thesis, data from remote networks in developing countries can be analyzed with the new methods. So far, the methods focus on investigation of 3-phase networks but show potential to be applied to single phase networks, too. For long terms, the methods are meant to be the basis of a portable power quality analyzer. For this purpose, it would be advantageous to be able to investigate single-phase as well as three-phase networks. Besides that, also the real-time application of the EMD needs to be promoted.

During the work on the thesis, further promising applications of the EMD in electrical networks have been discovered:

- Separation of modes for calculation of positive, negative and zero sequences in 3-phase systems
- Replacing linear filter, used in Phase Locked Loops.
- Separation of average and oscillating power for Shunt Active Compensators.

For these applications, it needs to investigate if the delay through computational afford is shorter or worse than the phase shift property of linear filters. The real-time EMD version is essential for taking advantage of the developed methods in grid-connected equipment.

Bibliography

[1] AsianDevelopmentBank. Bhutan: Energy sector, eveluation study. *Reference Number: SAP BHU 2010-21*, 2010.

[2] Geir Kulia. Investigation of distortions in microgrids. Master's thesis, Norwegian University of Science and Technology, October 2016.

[3] Hï¿œkon Duus. An integrated tool for microgrid design in rural areas. Master's thesis, Norwegian University of Science and Technology, November 2015.

[4] WorldHealthOrganization. Access to modern energy services for health facilities in resource-constrained settings. ISBN: 978 92 4 150764 6, 2014.

[5] John H. Barton. Intellectual property and access to clean energy technologies in developing countries. an analysis of solar photovoltaic, biofuel and wind technologies. Technical report, International Centre for Trade and Sustainable Development (ICTSD), 2007.

[6] Norden E. Huang, Zheng Shen, Steven R. Long, Manli C. Wu, Hsing H. Shih, Quanan Zheng, Nai-Chyuan Yen, Chi Chao Tung, and Henry H. Liu. The empirical mode decomposition and the hilbert spectrum for nonlinear and non-stationary time series analysis. *Proceedings of the Royal Society of London*, 1998. doi: 10.1098/rspa.1998.0193.

[7] Jan Machowski, Bialek Janusz W., and Bumby R. James. *Power System Dynamics, Stability and Control*. John Wiley & Sons, Ltd, 2008.

[8] T.C. Green and M. Prodanovic. Control of inverter-based microgrids. *ELECTRIC POWER SYSTEMS RESEARCH*, 2007. doi: 10.1016/j.epsr.2006.08.017.

[9] Joan Rocabert, Alvaro Luna, Frede Blaabjerg, and Pedro Rodrï¿œguez. Control of power converters in ac microgrids. *IEEE Transactions on Power Electronics*, 27(11):4734 – 4749, November 2012. doi: 10.1109/TPEL.2012.2199334.

[10] Yong Chen, Ralf Hesse, Dirk Turschner, and Hans-Peter Beck. Investigation of the virtual synchronous machine in the island mode. *IEEE PES Innovative Smart Grid Technologies Europe*, 2012. doi: 10.1109/ISGTEurope.2012.6465648.

[11] Salvatore D'Arco, Jon Are Suul, and Olav B. Fosso. A virtual synchronous machine implementation for distributed control of power converters in smartgrids. *Electrical Power System Research*, 2015. doi: 10.1016/j.epsr.2015.01.001.

[12] Michael Taylor, Pablo Ralon, and Andrei Ilas. The power to change - solar and wind cost reduction potential to 2025, 2016. URL `www.irena.org/DocumentDownloads/Publications`. IRENA.

[13] Yoshihiko Wazawa. Analysis and forecast of pv power variation. Technical report, Chubu Electric Power Co., Inc., October 2012.

[14] Hugo Lucas, Salvatore Vinci, and Divyam Nagpal. Iorec 2012 international off-grid renewable energy conference, key findings and recommendations. Technical report, IRENA, 2012.

[15] Salvatore Vinci, Divyam Nagpal, Troy Hodges, and Rabia Ferroukhi. Accelerating off-grid renewable energy, iorec 2014: Key findings and recommendations. Technical report, IRENA, 2014.

[16] Ned Mohan, Tore M. Undeland, and William P. Robbins. *Power Electronics, Converters, Applications and Design*. John Wiley & Sons, Inc., third edition edition, 2003.

[17] F.J. Harris. On the use of windows for harmonic analysis with the discrete fourier transform. *Proceedings of the IEEE*, 66, Januar 1978. doi: 10.1109/PROC.1978.10837.

[18] Inc. Maxim Integrated Products. Tutorial 1040 - coherent sampling vs. window sampling, March 2002. URL `https://www.maximintegrated.com/en/app-notes/index.mvp/id/1040`.

[19] Tomasz Tarasiuk. Angular frequency variations at microgrids and its impact on measuring instruments performance. *IET Generation, Transmission & Distribution*, 2016. doi: 10.1049/iet-gtd.2015.1572.

[20] Hirofumi Akagi. *Instantaneous Power Theory and Applications To Power Conditioning*. Wiley, 2007.

[21] Oliver Grillmeyer. *Exploring Computer Science with Scheme*. Springer, 1998. learning rate is discussed on page 506.

[22] Zhaohua Wu and Norden E. Huang. Ensemble empiciral mode decomposition: A noise assisted data analysis method. *Advances in Adaptive Data Analysis*, 01(01):1–41, 2009. doi: 10.1142/S1793536909000047.

[23] Ryan Deering and James F. Kaiser. The use of a masking signal to improve empirical mode decomposition. *ICASSP*, 2005. doi: 10.1109/ICASSP.2005.1416051.

[24] Tomasz Tarasiuk. Estimator-analyzer of power quality, part i methods and algorithms. *Journal of the International Measurement Confederation*, 2010. doi: 10.1016/j.measurement.2010.09.049.

[25] Tomasz Tarasiuk, Mariusz Szweda, and Marcin Tarasiuk. Estimator-analyzer of power quality, part ii hardware and research results. *Journal of the International Measurement Confederation*, 2010. doi: 10.1016/j.measurement.2010.09.048.

[26] Salvatore D'Arco, Jon Are Suul, and Marta Molinas. Implementation and analysis of a control scheme for damping of oscillations in vsc-based hvdc grids. *16th International Power Electronics and Motion Control Conference and Exposition*, 2014. doi: 10.1109/EPEPEMC.2014.6980558.

[27] G.Gabriel Rilling and Patrick Flandrin. One or two frequencies? the empiciral mode decomposition answers. *IEEE Transactions on Signal Processing*, 2008. doi: 10.1109/TSP.2007.906771.

[28] R. T. Rato, Manuel Duarte Ortigueira, and Arnaldo Guimarï¿œes Batista. On the hht, its problems, and some solutions. *Mechanical Systems and Signal Processing*, 2008. doi: 10.1016/j.ymssp.2007.11.028.

Appendix A

Line- to Phase Voltage Transformation

This appendix contains the derivation of matrices that can be used to transform line-voltages v_{ab}, v_{bc} and v_{ca} into phase-voltages v_a, v_b and v_c. Different approaches are possible to obtain similar results.

The discussion about the advantages and disadvantages of each matrix is conducted as a follow up to the derivation within this Appendix.

$$v_{ab} = v_a - v_b \tag{A.1}$$

$$v_{bc} = v_b - v_c \tag{A.2}$$

$$v_{ca} = v_c - v_a \tag{A.3}$$

$$v_a + v_b + v_c = 0 \tag{A.4}$$

When real measurements are assumed, the following equation, considering a random error on each line-voltage (e_{ab}, e_{bc} and e_{ca}), can be set up:

$$v_{ab} + e_{ab} = v_a - v_b \tag{A.5}$$

$$v_{bc} + e_{bc} = v_b - v_c \tag{A.6}$$

$$v_{ca} + e_{ca} = v_c - v_a \tag{A.7}$$

Approach 1

The calculation of each phase voltage is done in 2 steps. First, the two line-voltages that contain the respective phase voltages are subtracted from each other. Afterwards equ. A.4 is rearanged and used to eliminate the phase voltages that are not in focus.

Equ. A.8, A.9 and A.10 show the results for the 3 phase-voltages.

$$v_a = \frac{1}{3}v_{ab} - \frac{1}{3}v_{ca} - \frac{1}{3}(e_{ca} - e_{ab}) \tag{A.8}$$

$$v_b = -\frac{1}{3}v_{ab} + \frac{1}{3}v_{bc} - \frac{1}{3}(e_{ab} - e_{bc}) \tag{A.9}$$

$$v_c = -\frac{1}{3}v_{bc} + \frac{1}{3}v_{ca} - \frac{1}{3}(e_{bc} - e_{ca}) \tag{A.10}$$

Matrix A.11 summarizes the results for all three phases. This matrix can be used in equ. 2.18 of chapter 2.4.

$$M = \begin{bmatrix} \frac{1}{3} & 0 & -\frac{1}{3} \\ -\frac{1}{3} & \frac{1}{3} & 0 \\ 0 & -\frac{1}{3} & \frac{1}{3} \end{bmatrix} \tag{A.11}$$

The sum of the phase voltages results to zero, as the elements from equ. A.8, A.9 and A.10 cancel out. Approach 1 distributes the line-voltages equally so that every phase voltage consists of a similar big part of the two line-voltages that comprises it.

Approach 2

This is an approach that holds mathematical correctness with flawless data but shows disadvantage when it is applied to real measurements. Measurement errors are not evenly distributed among the phase-voltages.

The procedure starts with rearranging equ. A.4 to eliminate one of the phase voltages in equation A.5, A.6 or A.7. Followed by rearranging the resultant equation and inserting it in the respective other phase-voltage definitions two more times, the unknown phase-voltages can be obtained. Depending on the order in which the inserting takes place, different matrices result.

Equ. A.12 shows an example case of transformation according to approach 2.

$$\begin{aligned} v_a &= -\tfrac{1}{3}v_{ab} - \tfrac{2}{3}v_{bc} - v_{ca} - \tfrac{1}{3}e_{ab} - \tfrac{2}{3}e_{bc} - e_{ca} \\ v_b &= -\tfrac{1}{3}v_{ab} + \tfrac{1}{3}v_{bc} - \tfrac{1}{3}e_{ab} + \tfrac{1}{3}e_{bc} \\ v_c &= -\tfrac{1}{3}v_{ab} - \tfrac{2}{3}v_{bc} - \tfrac{1}{3}e_{ab} - \tfrac{2}{3}e_{bc} \end{aligned} \tag{A.12}$$

In total 6 different orders are possible, which each result into a different matrices. Mathematically they can be proven to be equalent if balanced line-voltages (equ. A.13) are assumed. Remarkable is, that always one of the lines is equal to a respective line of matrix A.11 from approach 1. In equation A.14 all possible

matrices from approach 2 are shown. M_2 corresponds to the example case from A.12.

$$v_{ab} + v_{bc} + v_{ca} = 0 \tag{A.13}$$

$$M_2 = \begin{bmatrix} -\frac{1}{3} & -\frac{2}{3} & -1 \\ -\frac{1}{3} & \frac{1}{3} & 0 \\ -\frac{1}{3} & -\frac{2}{3} & 0 \end{bmatrix} \quad M_3 = \begin{bmatrix} 1 & \frac{2}{3} & \frac{1}{3} \\ 0 & \frac{2}{3} & \frac{1}{3} \\ 0 & -\frac{1}{3} & \frac{1}{3} \end{bmatrix} \quad M_4 = \begin{bmatrix} \frac{1}{3} & 0 & -\frac{1}{3} \\ \frac{1}{3} & 1 & \frac{2}{3} \\ \frac{1}{3} & 0 & \frac{2}{3} \end{bmatrix}$$

$$M_5 = \begin{bmatrix} \dots \\ \\ \end{bmatrix} \quad M_6 = \begin{bmatrix} \dots \\ \\ \end{bmatrix} \quad M_7 = \begin{bmatrix} \dots \\ \\ \end{bmatrix} \tag{A.14}$$

The sum of the phase voltages is equal to the negative sum of the line-voltages inklusive their measurement error. Equ. A.15 shows this relationship. It can be derived from any of the 6 matrices. The sum of the (true and balanced) phase voltages equals to zero but the errors do not cancel each other out.

$$v_a + v_b + v_c = -\cancelto{0}{(v_{ab} + v_{bc} + v_{ca})} - (e_{ab} + e_{bc} + e_{ca}) \tag{A.15}$$

Appendix B

Phase Locked Loop Implementation

This appendix shows the PLL that is developed by D´Arco et al. [26] and implemented in Matlab/Simulink. For the means of the thesis, the parameters are empirically tuned. The Matlab code sets parameters and calls the Simulink model that is shown in fig. B.1.

```
%% Run the PLL on Ship Measurements
% "Implementation and Analysis of a Control Scheme for Damping of
% Oscillations in VSC-based HVDC Grids"
% DOI: 10.1109/EPEPEMC.2014.6980558
%
% ... that was implemented in Simulink
%
% Benedikt Hillenbrand, 23.05.2017

% Import of all data (20,064,000 samples - 668,8s)
load('CompensatedMeasurements_11m.mat')
% Preparation of the data for the Simulink model
n = 1800000;   % ADJUST number of imported samples (max: 20,064,000)
Vab = Vab_11m(1:n,1); clear Vab_11m;
Vbc = Vbc_11m(1:n,1); clear Vbc_11m;
Vca = Vca_11m(1:n,1); clear Vca_11m;
time = time(1,1:n); t_end = n/sampleRate;

V_abc=[Vab'; Vbc'; Vca'];
V_abcTimeSeries=timeseries(V_abc',time);

%% PLL & Park Transformation
W_LP_PLL = 200;
sim('PhaseLockLoop_salvatore.slx');
% Results from the simulation
w_PLL       = w_PLL_Salvatore.Data';
theta_PLL   = theta_PLL_Salvatore.Data';
V_park(1,:) = Xd.Data;  V_park(2,:) = Xq.Data;
```

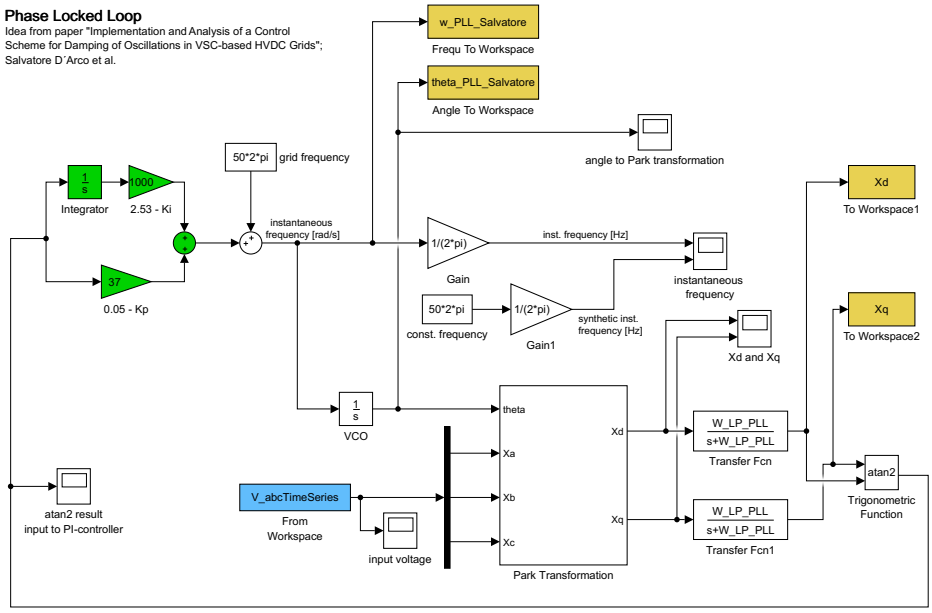

Figure B.1: Simulink Modell of the PLL implementation